

**REVIEW OF AERONAUTICAL FATIGUE
INVESTIGATIONS IN JAPAN
DURING THE PERIOD JULY 2005 TO MAY 2007**

Edited by
Hiroyuki Terada
Japan Aerospace Technology Foundation

and

Nobuo Takeda
The University of Tokyo

For Presentation at the 30th Conference of
the International Committee on Aeronautical Fatigue

Naples, Italy, 14-15 May 2007

Contents

	page
12.1 INTRODUCTION	12/4
12.2 LIFE EVALUATION ANALYSIS	12/5
12.2.1 Inspection Schedule for Fatigue Sensitive Aircraft Structure by Hybrid Bayesian Analysis Code	12/5
12.3 FATIGUE IN METALLIC MATERIALS AND COMPONENTS	12/6
12.3.1 Evaluation of Properties for Friction Stir Welded Butt Joint in 2024-T3 Aluminum Alloy	12/6
12.3.2 Improvement of Crack Propagation Properties of Friction Stir Welded Panel	12/8
12.3.3 Application Study of Fatigue Improvement by Laser Peening for Life Limited Dynamic Components	12/9
12.4 FATIGUE IN COMPOSITE MATERIALS AND COMPONENTS	12/10
12.4.1 Evaluation of Mode I Crack Suppression Method for Foam Core Sandwich Panel with Fracture Toughness Test and Analyses	12/10
12.4.2 Effects of Water Absorption and Thermal Environment on Compression after Impact (CAI) Characteristics of CFRP Laminates	12/11
12.4.3 Development and Full Scale Static Test of Low-Cost Composite Wing Demonstrator with VaRTM Process	12/12
12.4.4 Descriptive Relationships between Bearing Response and Damage Progression in Bolted Composite Joints	12/14
12.4.5 A New Approach to Determine Damage Growth in Bolted Composite Joints	12/16
12.4.6 A-VaRTM for Primary Aircraft Structures	12/19
12.5 FULL-SCALE TESTING	12/20
12.5.1 US-1A KAI Full-Scale Fatigue Test	12/20
12.5.2 P-X/C-X Full-Scale Structural Strength Test	12/21
12.5.3 Structural Substantiation of Unmanned Supersonic Experimental Airplane for Vibratory Loading	12/22

12.6 STRUCTURAL HEALTH MONITORING	12/24
12.6.1 Structural Health Management of Composite Structures Using Small-Diameter Fiber Optic Sensors	12/24
12.6.2 Structural Health Monitoring of Composite Wing Structure during Durability Test	12/25
12.7 AIRCRAFT ACCIDENT INVESTIGATION	12/27
12.7.1 Aircraft Accident Investigation and Aircraft Serious Incident Investigation	12/27
12.8 ICAF DOCUMENTS DISTRIBUTED BY JAPAN DURING 2005 TO 2007	12/28
ACKNOWLEDGEMENTS	12/28
TABLES AND FIGURES	12/29

12.1 INTRODUCTION

Hiroyuki Terada, National Delegate, Japan Aerospace Technology Foundation

This review covers the research activities on aeronautical fatigue and related topics conducted by Japanese research laboratories, universities and industries.

The organizations and number of reports submitted to the review were as follows:

- Japan Aerospace Exploration Agency (JAXA) (8)
- Technical Research and Development Institute, MoD (TRDI) (2)
- Aircraft and Railway Accident Investigation Commission (ERAIC) (1)
- Mitsubishi Heavy Industries, Ltd. (MHI) (2)
- Kawasaki Heavy Industries, Ltd. (KHI) (1)
- Fuji Heavy Industries, Ltd. (FHI) (1)
- The University of Tokyo (1)

Before describing the research activities, the author would like to introduce the general activities on aircraft development program in Japan during 2005 to 2007.

International Cooperation:

Under the mutual understanding established in 1970 between Japan and the US, Japanese major aircraft manufacturers (MHI, KHI, FHI and Japan Aircraft Development Corporation (JADC)) and the Boeing signed MOA on the development of the B-787, Dreamliner, in October 2004. Formal contract detailing the work share was signed in May 2005. According to the agreement, Japanese firms share approximately 35% of the B-787 structures. Figure 12.1 shows the total work share of the structures.

Japanese industries have also participated in the development of Airbus A380 as the subcontractor or the supplier since October 2004. Portion of parts supplied from Japanese industries in A380 Program is presented in Figure 12.2.

Domestic Developments:

Development of MJ-90, the regional jet for 90 passengers, is under way at MHI expecting to obtain Type Certificate (TC) in 2012. The main target is to achieve higher fuel efficiency compared with the similar class fleet now in operation (see Figure 12.3). The strong points of the aircraft are low cost and lightweight using plenty of composite structures by VaRTM technologies, clean exhaust and low noise.

Development Program of next Patrol aircraft (P-X) and Cargo aircraft (C-X) are under way expecting the first flight in 2007 for both aircraft. Production of prototype aircraft is in progress with Kawasaki Heavy Industries as the prime contractor.

Development of improved modification type of US-1A, the amphibian aircraft, for search and rescue and also fire fighting is also under way, together with the marketing surveillance. Some details are described in each article.

YS-11, the Japanese middle range turboprop transport, manufactured 182 aircraft since 1962, finished its last flight as the airliner transport in Japan on September 30, 2006. No accidents caused by structural fatigue were reported during the whole operation of the fleet. Some of the retired aircraft are to be provided to the studies to enhance the safety of future aircraft at JAXA IAT (Japan Aerospace Exploration Agency, Institute of Aerospace Technology).

12.2 LIFE EVALUATION ANALYSIS

12.2.1 Inspection Schedule for Fatigue Sensitive Aircraft Structure by Hybrid Bayesian Analysis Code

Seiichi Ito*, Takao Okada* and Bintuan Wang **

* Japan Aerospace Exploration Agency (JAXA)

** The First Aircraft Institute of AVIC-I (China)

The purpose of this study is to perform reliability analysis for developing an optimal non-periodic inspection schedule and estimating values of uncertain parameters from the field data collected during in-service inspections for aircraft structural elements. These functions are applied to the hybrid Bayesian analysis code (HYBAC) which is a combination of the conventional Bayesian method and fuzzified Bayesian analysis. The Bayesian reliability analysis that can rationally estimate the characteristics of uncertain parameters of the structure is very useful tool to deal with sparse data. Bayesian approach is appropriate for use in the reliability analysis because they are derived from the framework of subjective probability. In addition, the fuzzified Bayesian method is also considered by the use of structural operation data obtained from inspection results which often comprise subjective information. The hybrid Bayesian approach proposed in this paper is unique and novel in that it allows one to utilize judiciously the results of earlier inspections for the purpose of determining the time of

the next inspection and estimating values of several parameters involved in the problem that can be treated as uncertain. Numerical simulations for a transport wing lower surface structure verify the above-mentioned capabilities of the HYBAC. The structure of hybrid Bayesian analysis code(HYBAC) for structural reliability evaluation is given in Figure 12.4

12.3 FATIGUE IN METALLIC MATERIALS AND COMPONENTS

12.3.1 Evaluation of Properties for Friction Stir Welded Butt Joint in 2024-T3 Aluminum Alloy

Takao Okada*, Toshiya Nakamura*, Shigeru Machida* and Motoo Asakawa**

* Japan Aerospace Exploration Agency (JAXA)

** Waseda University

Friction Stir Welding (FSW) invented by TWI in 1991 is a relatively novel joining technique and there are many research activities for evaluation of properties for FSW. Its application spreads in many structures such as automobiles, trains, rockets, ships and so on. For civil aircraft, Eclipse aviation firstly obtained FAA Type Certificate to their business jet Eclipse500 in 2006 and other companies plan to employ FSW for transport category aircraft¹⁾,²⁾. Then the way to comply with damage tolerance requirement for FSW structure is one of the intensive research activities.

However, some research works point out that damage tolerance requirement is not sufficient to establish structural integrity of aircraft structure operated in environmental circumstance. In damage tolerance requirement, structural design allowables are usually not adjusted for corrosion effects except for environmental influences on fatigue crack propagation. But degradation of fatigue life under corrosive environment has been widely known and it has recently been investigated that the selection of initial discontinuity size and corrosion scenarios has a large effect for the evaluation of fatigue life and decisions related to inspection intervals.

Therefore holistic life prediction including the effect of environment and heterogeneity of the material is imperative to provide the necessary structural integrity for aircraft structure³⁾. In this method a subset of the Initial Discontinuity State (IDS) / Modified Discontinuity State (MDS) acts as crack nucleation site. Based on this circumstance and the progress in engineering technology, research for IDS of the material used in aircraft structure is conducted⁴⁾. In case of FSW joint, the microstructure in its joint is different from that in base

material. Treatment of the tool mark and burr during FSW process is different depending on the applied location. And type of the joint such as butt, shear lap or hard point and etc. may change the crack nucleation site of the joint. Then investigation of IDS in FSW joint also seems to be important to provide structural integrity for aircraft structure. In addition, evaluation of short crack growth behavior in FSW joint is imperative to establish holistic life prediction. Then micro- and macrostructure, fatigue properties and crack nucleation site under fatigue loading are evaluated.

FSW butt joint in 2024-T3 Aluminum alloy is used for evaluation. Rolling direction of the plates is parallel to the direction of friction stir weld. The thickness of the plates before joining is 2.0mm.

Figures 12.5 and 12.6 show the section perpendicular to the welding line and parallel to it, respectively. The feature for perpendicular section is close to that reported in other papers. The periodic feature is observed on the section parallel to the welding line. It is found that the measured pitch of the tool mark and that of the periodic feature are same as the ratio of the tool traveling speed to the tool rotation speed. This tendency is also observed other joining condition.

Specimen with tangentially blended fillets is used for the fatigue test. Specimens are cut out from the panel so that direction of friction stir weld is perpendicular to the loading direction and its joined line locates at the center of the specimen. Therefore the specimen is loaded in T-direction. To exclude the effect of tool mark and burr on crack nucleation, both surfaces of the specimen are first ground and then polished with diamond paste up to $0.3\mu\text{m}$. Same preparation is applied to both sides of the specimen to prevent crack nucleation from its sides. The width of the specimen and its final thickness is about 9.2 and 1.85mm, respectively. The specimens are subjected to cyclic loading with $R=0.1$, $f=10\text{Hz}$ and $\sigma_{\text{max}}=200\text{MPa}$. The test is conducted at room temperature. Fatigue tests are stopped at several intervals to capture cracks.

At about 650,000 cycles, two adjacent cracks are observed on the back surface of the specimen. Total crack length is about 1.2mm. These cracks are located mostly at the center for loading direction. Then without surface roughness such as the tool mark and burr, Heat Affected Zone (HAZ) and Thermo-Mechanically Affected Zone (TMAZ) are not act as crack nucleation site in this case. And because of these locations, the kissing bond may be nucleation sites. Metallographic observation of this specimen will be conducted to confirm this assessment. And effect of surface finish on crack nucleation site is planed to evaluate.

References

- 1) M. Pacchione and S. Werner, "Welding of Fuselage Structure", Review of Aeronautical

- Fatigue Investigations in Germany During the Period March 2003 to May 2005, pp. 34-35.
- 2) H. Sato, et. al, "Fatigue and Crack Propagation Properties of Friction Stir Welded Lap Joint and Panel", Presented at ICAF2005.
 - 3) D. W. Hoepfner, "From Safe Life to Holistic Structural Integrity Design, A journey in aircraft design evolution", Presented at NRC, 2002.
 - 4) A. Merati, "A study of nucleation and fatigue behavior of an aerospace aluminum alloy 2024-T3", International Journal of Fatigue, Vol. 27, 2005, pp. 33-44.

12.3.2 Improvement of Crack Propagation Properties of Friction Stir Welded Panel

Hiroaki Sato, Yosuke Yamada, and Yoshitsugu Tanoue

Mitsubishi Heavy Industries, Ltd. (MHI)

Friction stir welding is the one of the advanced joining methods for aircraft manufacturing. In the last report, which was presented at ICAF 2005, crack propagation properties of FSW joints were evaluated using coupon specimens and sub-component structures. Crack propagation properties were strongly affected by residual stresses due to FSW. Tensile residual stresses accelerated the crack growth, and compressive residual stresses suppressed the crack growth. These crack growth behaviors can be explained by the linear fracture mechanics, which is used for the conventional welded structures.

In this study, the crack propagation properties were evaluated by using the panel of five stringers with initial cracks, which is shown at Figure 12.7. The crack propagation properties of FSW and riveted panels are shown at Figure 12.8. The crack propagation speed of FSW panel is much faster than that of riveted panels. The crack propagation time from visible size crack (50.8mm) to critical crack length of FSW panel is 1/3 of that of the riveted panel. The crack propagation of the FSW panel is accelerated by the tensile residual stress due to FSW and the crack propagation from skin to stringers. The cracks, initiated at skin, propagated directly to the center stringer, and the center stringer was broken before the skin crack did not become so large. Then the center stringer was unable to stiffen the panel, the skin crack propagation speed became faster. So the crack propagation properties of FSW panel are inferior to those of riveted panels.

To improve the crack propagation properties of the FSW panel, the reduction of residual stress is very effective. The stress relief temperature of aluminum alloy is normally higher than the aging temperature. So the heat treatment after FSW cannot reduce the residual stress without strength reduction. The residual stress after welding is due to the shrinkage of weld metal. If the shrunk metal is stretched, the residual stress will be released. To release the

residual stress, the roller burnishing method was used in this study. The center of FSW area was burnished by the hard coated metallic roller, the residual stress distribution at FSW area was changed.

The crack propagation properties of FSW coupon specimens after the burnishing treatments were evaluated. The crack propagation properties of those specimens depended on the burnishing conditions. In case of good burnishing condition, the crack propagation properties are better than those of riveted joints. The FSW panels with the burnishing treatment were also evaluated in this study. The test results are shown at Figure 12.9. And we have found that this method is very effective to improve the crack propagation properties of FSW panel.

This study was supported by METI and NEDO, Japan.

12.3.3 Application Study of Fatigue Improvement by Laser Peening for Life Limited Dynamic Components

Hiroshi Taguchi, Masahiro Obukata, Takafumi Adachi, Toshimichi Ogisu and Masakazu Shimanuki

Fuji Heavy Industries Ltd. (FHI)

Laser peen process is a new surface treatment technique for strengthening metals. Recently the laser peening technique is rapidly advancing in conjunction with laser technology development.

In this study, establishing process parameters for 7000 series aluminum alloy, coupon fatigue test and actual-sized element test were conducted, and the fatigue characteristics improvements by the laser peening were demonstrated.

The optimization of the laser peen process parameters, such as laser pulse energy, laser pulse duration, focal spot size and so on were evaluated by the residual stress distribution, and the surface roughness. The maximum compressive residual stress by laser peening has achieved more than double of compressive residual stress by shot peening. The roughness of laser peened surface is smoother than Ra 6.3 micro meter.

After establishing process parameters, coupon fatigue tests for un-notched specimens and flat plate with a central circular hole specimens were conducted. Figure 12.10 shows that the fatigue life of un-notched laser peened specimens are enhanced more than three times of shot peened specimens. The flat plate with a central circular hole specimens were used for evaluating the fatigue characteristics improvement on condition of the stress concentration.

The enhancement of fatigue life of flat plate with a central circular hole was greater than the enhancement of un-notched specimen.

The actual-sized element test specimen was simulated as a pitch horn. The pitch horn is a part of flight control system for the main rotor of helicopter (see Figure 12.11). The pitch horn in actual helicopter is loaded by about 5Hz high cycle fatigue load during flight, then the retirement life is assigned to this part because of fatigue damage during operation. The actual-sized element test was conducted by applying simple sinusoidal load, as shown in Figure 12.12. The laser peened specimen showed the fatigue enhancement compared with untreated specimen.

The cost study considering both lifetime extension and cost of laser peen process was conducted and 20% cost reduction compared with untreated parts was estimated.

12.4 FATIGUE IN COMPOSITE MATERIALS AND COMPONENTS

12.4.1 Evaluation of Mode I Crack Suppression Method for Foam Core Sandwich Panel with Fracture Toughness Test and Analyses

Yasuo Hirose*, Go Matsubara*, Hirokazu Matsuda*, Fumihide Inamura*, and Masaki Hojo**

* Kawasaki Heavy Industries, Ltd. (KHI)

** Kyoto University

A new type of crack arrester was proposed for an interfacial crack between a facing and a core for a CFRP / foam core sandwich panel based on the behavior that the interfacial crack in the foam core sandwich panel remained between the surface skin and the foam core. It was considered that the dissimilar material with higher stiffness on the crack propagation path would suppress crack propagation. The concept of the crack arrester is shown in Figure 12.13. This report describes the analytical prediction and experimental validation of this concept in the mode I type loading condition.

Finite element calculations were carried out to evaluate the driving force of the interfacial crack using fracture mechanics parameters. Here, the energy release rates were calculated under mode I type loading conditions with FE models of test specimen configurations. These energy release rates with and without the crack arrester were compared. Loading condition of the test specimen is shown in Figure 12.14.

A considerable reduction of the energy release rates at the crack tip was confirmed in

the FE analyses as the crack tip approached the crack arrester. The energy release rate at the crack tip was abruptly reduced starting at a point of 15 mm from the leading edge of the crack arrester and converged to a small value close to zero near the arrester edge. The relation between normalized energy release rate and distance L is shown in Figure 12.15. In this figure, “Normalized energy release rate” is defined as a ratio between the energy release rate with a crack arrester and that without an arrester (using the same crack length). Distance L is also defined as the length between the leading edge of the crack arrester and the crack tip.

The verification test was conducted and test results indicated that a crack arrester increased the critical load of the test specimen for mode I type loading. On the other hand, the critical load of the specimen without crack arrester decreased in a stick slip manner. The relation between critical load and cross head displacement is shown in Figure 12.16. Apparent energy release rates were calculated with a crack closure method using FE analyses data and the interfacial fracture toughness value derived from test data of the specimen without a crack arrester. Apparent energy release rates with and without a crack arrester are shown in Fig. 12.17 Through this comparison, an approximately 5 times increase to the energy release rate near the arrester edge was obtained due to the crack arrester.

Through these studies, the effect of the crack arrester under mode I type loading was predicted analytically and evaluated experimentally.

12.4.2 Effects of Water Absorption and Thermal Environment on Compression after Impact (CAI) Characteristics of CFRP Laminates

Yuichiro Aoki*, Ken Yamada**, and Takashi Ishikawa*

* Japan Aerospace Exploration Agency (JAXA)

** MAZDA Motor Corporation

Effects of water absorption and thermal environment on compression after impact (CAI) characteristics of CFRP laminates were studied. The T800/3633 carbon fiber/epoxy laminate manufactured by Toray Industries, Inc. were used in this study, which is generally used for various aircraft structure. This material system also had a large amount of available basic material data obtained by our facility that is now available on internet website of Japan Aerospace Exploration Agency (JAXA).

Specimens were immersed in 71 °C water for 10,000 hours (410 days) to quantify the ratio of water absorbed in the CFRP laminates. Water gain of the specimen was 1.4wt% after the

water absorption test. Numerical simulation using FEM code was conducted to predict moisture diffusion based on the measured orthotropic diffusion constants. Then impact tests by the drop-weight were carried out at room temperature at normalized energy level of 3.3 J/mm. Compression tests after impact were carried out at various temperatures, i.e., 25 °C (RT: Room Temperature), 82 °C, 177 °C, for water absorbed specimens, and -54 °C, RT, 82 °C, 121 °C, 149 °C, 177 °C for dry specimens. After impact test, the size and shape of damages were inspected by the ultrasonic C-scan system for all specimens. Some of specimens were cut into slices by a diamond fine saw to obtain the cross-sectional damage state. From the observation, it was found that delamination area and the number of transverse cracks of the water absorbed CFRP were smaller than those of dry specimens. Figure 12.18 summarizes the CAI strengths of dry and water absorbed specimens at various temperatures and indicates reference information of interlaminar fracture toughness taken from JAXA advanced composite database system. Several important findings are indicated in this figure where two or three CAI data are included at each temperature point. The first point is that CAI strengths are well correlated with mode II fracture toughness at least from the RT to mid-high temperature of 121 °C. The second finding is that CAI strengths of wet specimens are slightly higher than those of dry specimens. This result implies that the size of delamination mentioned above governs CAI strength. The third finding is a serious decrease of CAI strength in wet specimen at 177 °C that is most impressive result of the present study. According to the measurement of the glass transition temperature (T_g), it was decreased to 124 °C for the water absorbed specimen while the T_g of dry specimen is 174 °C. Thus, the tested temperature of 177 °C for compression is quite high and then the compressive strength of composite laminate was almost lost. Ultrasonic C-scan results taken after compressive failure shown in Fig. 12.19 can well explain the discussion above. In the case of 177 °C wet CAI test, impact induced delamination was not the trigger of the failure. Instead, buckling induced crippling type of failure was observed. These findings must be important and helpful information to understand the overall CAI behavior under environmental conditions. This test continues today and compression tests of wet specimen at the mid-high temperature range from 121 °C to 149 °C are being conducted.

12.4.3 Development and Full Scale Static Test of Low-Cost Composite Wing Demonstrator with VaRTM Process

Yoshiyasu Hirano, Yuichiro Aoki, Yutaka Iwahori, and Yosuke Nagao
Japan Aerospace Exploration Agency (JAXA)

JAXA has been involved in the research and development of the technologies needed for low-cost, light-weight composite structures for commercial aircraft. Because of their potential for reducing the weight and manufacturing cost, VaRTM (Vacuum-Assisted Resin Transfer Molding) graphite/epoxy material system is now focused on. Since the VaRTM process does not require expensive materials and manufacturing equipments such as conventional prepreg and autoclave systems, it offers the potential to reduce manufacturing costs. However, because of the low pressure condition during the cure cycle, it is difficult to achieve high mechanical properties and a high fiber volume fraction using the conventional VaRTM process. Therefore, it is necessary to develop a novel VaRTM process to guarantee higher mechanical properties and more stable quality for aircraft structures.

The step-by-step development of the VaRTM aircraft structure has been conducted based on a building block approach and many tests have been done at each step to evaluate the formability and mechanical properties of the material.

First, many types of coupon tests are performed for several kinds of dry preform and resin in order to evaluate mechanical properties. As a consequence of this effort, the newly developed VaRTM graphite/epoxy material achieves high mechanical properties and high fiber volume fraction of 56.5% on average. The results of the coupon tests of NHT, OHT, NHC, OHC and CAI are summarized in Figure 12.20.

The formability is evaluated by manufacturing the three types of demonstrators: (a) the 2m long stiffened panel, (b) the 2.1m long wing structure, and the third demonstrator of (c) 6m long full-scale wing structure (See Figure 12.21).

The 2 m × 1 m flat stiffened panel (a) has two different shapes of stringers: Z-shape and hat-shape. This panel was successfully fabricated integrally by VaRTM process. Then, the second demonstrator (b) of the 2 m long integral structure consist of a curved stiffened skin panel and spars was manufactured to simulate an outer wing of a mid-size civil aircraft. Conventional blade type stringers were adopted. This demonstrator also includes some technical challenges, such as ply drop-off and a thick section around the access hole. As a result of the fabrication, incomplete resin impregnation or partial dry spots were found in the thick sections. They were attributed to the low permeability of the present dry preform. Then, some of the process parameters such as the locations of resin inlets and outlets, the flow sequence and impregnation time were carefully modified so that the resin can flow into the mold and fill the preform completely. Then, the third demonstrator (c) of the 6m long wing structure has been fabricated successfully with the improved fabrication process. Incomplete resin impregnations and partial dry spots were carefully checked by visual inspection and NDI; any defect was not detected.

Now, a number of mechanical property tests of sub-components and coupon specimens which obtained by cut-out from the 6m long demonstrator are planned in order to evaluate the manufacturing quality and the mechanical properties of a large-sized VaRTM structure.

Furthermore, the full scale static test of wing box fabricated from VaRTM graphite-epoxy material is planned as the final step of this project. (See Figure 12.22) This wing box represents the load-carrying wing box of a 30-passenger commercial aircraft. The upper and lower skin panels, the front and rear spars, and ribs are fabricated from VaRTM graphite-epoxy material, minimizing the number of mechanical fasteners needed to assemble the wing box. The wing box was designed to withstand associated with two flight conditions: 2.5G upbending and -1.0G downbending. The loads are introduced through 4 hydraulic actuator/load cell assemblies. Each actuator/load cell assembly is connected to the floor and to the wing box by using swivels which would allow the actuator to rotate as the wing box deforms. The hydraulic actuator control system, Aero ST produced by MTS, is adopted to control the loading, and the high frequency data acquisition systems produced by Kyowa Electronic Instruments Co., Ltd. and VXI Technology Inc. are adopted to record data from all instrumentation. The wing box will be subjected to a 50% DLL (Design Limit Load) test for the -1.0G and 2.5G flight conditions to verify accurate function of all components and instrumentation, followed by a 100% DLL test. Finally, the wing box will be subjected to a 100% DUL (Design Ultimate Load) test for the 2.5G flight condition.

Through these series of developments and tests, we hope to establish an ideal technology for applying low-cost composite materials to a commercial aircraft.

12.4.4 Descriptive Relationships between Bearing Response and Damage Progression in Bolted Composite Joints

Yi Xiao

Japan Aerospace Exploration Agency (JAXA)

Fiber reinforced polymer matrix composites (PMCs) have already proven to be useful in today's aircraft industry due to their lightweight properties. These structural components are often assembled using mechanically fastened joints, which poses a particularly challenging problem for engineering mechanic specialists. If the design for the mechanically fastened joints is inadequate, it not only becomes the primary source of failure in the composite structures, but also directly affects the durability and reliability of the aircraft structures.

The experimental and numerical studies described in this work were conducted in order to understand the strength and failure of mechanically fastened composite joints¹⁾. A detailed experimental investigation that clarified the relationship between bearing strength and damage

progression behavior in bolted composite joints will be summarized as following. Figure 12.23 illustrates the strength and damage characteristics determined by this study. Bearing failure induces a compressive damage accumulation process that can be classified into four stages: damage onset, damage growth, local fracture and structural fracture. Fiber micro buckling and matrix cracking appear to be the dominant modes for the onset of damage, while the final failure stage is dominated by out-of-plane shear cracks and delamination. The lateral constraints and the matrix "toughness" based on the laminate also influence the bearing failure and damage mechanisms. Moreover, the accumulation of damage resulted from fiber micro-buckling, fiber-matrix shearing and matrix compression failure in the individual laminate layers.

Numerical study focuses on developing a two-dimensional model that is capable of predicting the bearing failure and stiffness response for mechanically fastened composite joints. Bearing failure in laminated composites can be grouped into two basic in-plane failure modes: matrix compression and fiber compression-shear failure. Although through-thickness shear cracks and delamination are out-of-plane failure modes, they are beyond the scope of this work, and will not be considered in this study.

A complex approach based on combining the nonlinear shear elasticity theory with a continuum damage mechanics approach was utilized to represent the nonlinear material behavior during loading. Hahn and Tsai formulated the following nonlinear shear stress/strain relationship using high-order elasticity theory²⁾.

$$\varepsilon_{12} = G_{12}^{-1}\sigma_{12} + \alpha\sigma_{12}^3 \quad (1)$$

Equation (1) is then transformed into the following incremental form, which will be implemented in a finite element program.

$$\sigma_{12}^{(i+1)} = \frac{1 + 2\alpha(\sigma_{12}^{(i)})^3(\varepsilon_{12}^{(i+1)})^{-1}}{1 + 3\alpha G_{12}(\sigma_{12}^{(i)})^2} G_{12}\varepsilon_{12}^{(i+1)} \quad (2)$$

The damage accumulation criteria based on Hashin and Yamada-Sun's hybrid failure criteria were adopted and a degradation model for the damaged layers is proposed for the stress redistribution analysis. The relationship between the failure criteria and the damage variable is shown in Table 12.1 for each failure mode, where FV_i are the internal field variables representing the damaged status of the lamina.

The strength response and damage pattern simulation results were compared with experimental data. Figures 12.24 (a) and (b) display the comparison between the calculated

and experimentally determined load-displacement curves leading up to the ultimate failure. The predicted ultimate strength is within 6% of the measured strength for the IM-7/PIXA composites and within 12% for the IM600/Q133 composites. Overall, the predicted curves agree with the experimental data very well, not only in the initial damage stage, but also in the final structural failure stage for the joints for both materials. The comparison of the predicted damage growth patterns as a function of the applied load is depicted with a set of X-ray radiographs, as displayed in Fig. 12.25. The damage pattern on each layer was plotted for different damage modes, and the applied load was obtained from the reaction with the central node of the pin. The predicted damage progression qualitatively shows the similar damage growth tendencies between the numerical and experimental results.

In this study, firstly, a detailed experimental investigation was performed to evaluate the bearing strength and damage behavior of mechanically fastened joints of two composite systems (IM-7/PIXA and IM600/Q133). The relationships between the load-displacement curve, AE characteristics, and failure mechanism were examined. Correlations between the damage pattern and its progress were partially described by the AE signal activities. X-ray radiography and SEM photographs provided basic explanations of the bearing failure mechanisms. Secondly, the progressive failure model was proposed to simulate the response of laminated composite joints. This model predicts the composite joint's in-plane response and strength until final structural fracture, and the failure can be analyzed layer-by-layer, element-by-element, or mode-by-mode. The primary advantage of this damage model is that it can be implemented using the commercial finite element code ABAQUS, and a proprietary computer code do not have to be developed. Therefore, this method can be universally applied as a computational tool for joint design.

References

- 1) Xiao, Y. and Ishikawa, T. Bearing Strength and Failure Behavior in Bolted Composite Joints (Part I&II), *Compos Sci Technol*, 65, 2005, p. 1022.
- 2) Hahn HT. and Tsai SW. Nonlinear elastic behavior of unidirectional composite laminae, *Journal of Composite Materials* 1973; 7:102-118.

12.4.5 A New Approach to Determine Damage Growth in Bolted Composite Joints

Yi Xiao

Japan Aerospace Exploration Agency (JAXA)

One of the major problems associated with the use of mechanically fastened joints is that it can cause unavoidable stress concentration at the fastener holes. As a result, they are

frequent sources of failure in aircraft structures, and the general failure mode in fastener joints is the bearing failure. Although such damage is barely visible, any growth of this damage can severely degrade the mechanical properties and the load-carrying capability of the structural components; hence, early detection of such damages is a key element for preventing catastrophic failure and prolonging the life of aircraft structures.

Current available inspection methods for the joint are employing non-destructive evaluation (NDE) techniques, such as ultrasonic scan, X-ray and eddy current etc., to obtain an image of bearing damage. However, fasteners may have to be disassembled and re-assembled for inspection, which is inconvenient and inefficient for airline because it can cause significant downtime and incurs excessive expense. Therefore, the development in utilizing structural health monitoring (SHM) concepts has attracted significant attention to overcome the issues among the current inspection methods. The primary objective of this study is to address these issues and develop a more practical and convenient method to detect effectively the bearing damage for bolted composite or metallic joints. The efforts should focus on how to utilize the structural functionality that can monitor their own structural integrity¹⁾.

The concept of bolt gauge (BG) was defined of the bolt itself as a sensory unit, which has been proposed in earlier work²⁻³⁾. Only bond a strain gauge onto the surface of bolt head to monitor the bolt strain changes, which is possible to identify the state of bearing damage. The pivot of detection is to measure the changes of bolt tension due to out-of-plane compressive deformation that is directly related to the bearing damage. Therefore, carrying out the BG measurements can give easily information on the resistances of the lateral constraint in bolted joint, that allow for the detection and quantification of bearing damage. Overview of the BG-based bearing damage identification system is shown in Figure 12.26. This unique system will not need specific sensors, actuators, signal processors and controllers for damage detection.

Extensive tests using double lap bolted joint specimens are performed to verify and examine the concept, reliability and capability of BG for damage monitoring through the different case studies, including the effects of the material response, bolt clamp-up, joint geometry and loading history etc.

Figure 12.27 shows the bearing damage estimates by BG measurement obtained at the monotonic tensile tests for different material systems, called CFRP specimen and Al specimen. For any case, it can be found clearly that the response of BG output was related directly to the bearing damage and/or deformation. BG output can be obtained in a relatively stable development together with the response of bearing strength (P - δ curve) until the bearing

damage occurred, but once the bearing damage occurred, a sharp change in BG output and AE signal was observed. Simultaneously, non-linear behavior appeared in the load-displacement curve. Afterwards, the change of BG output as well as AE signal increased monotonously with hole elongation. Figure 12.28 shows the typical curves of the BG output versus the applied load for the case of CFRP specimen subjected to an initially applied torque of finger tight, 12~15, 30~35 kgf-cm, respectively. Figure 12.29 shows the BG output versus the applied load for various joint geometries, since the distinction between the failures is established largely by the joint geometry, particularly the width-to-diameter ratio, w/d or the edge-to-diameter ratio, e/d . From above, it was evident that the BG output has not been influenced by the change of the initial clamp-up levels or the joint geometry but only has been influenced at the generating time of the initial damage. Figure 12.30 shows the BG output versus the applied load for the case of CFRP specimen and Al specimen during the cyclic loading-unloading tests. The enveloping curve shows nearly unchanged in comparison with the monotonic tensile test. The unloading and reloading curves, however, show a somewhat unexpected behavior than the loading, because of the relationship of permanent strain. The results indicate that BG output did not depend on a load history, but can record the permanent strain received in the past.

A finite element analysis was performed to discuss the monitoring mechanisms. The finite element model was established with the commercial finite element package ABAQUS. Because of symmetry, a half of the middle lap in a double shear-lap bolted joint with one-half of the thickness of the aluminum plate was modeled. To predict the bearing damage responses in bolted aluminum plate joint, the progressive failure analysis and material degradation were performed. Since aluminum materials are highly nonlinear, they may also exhibit different yield stresses in tension and compression. Comparison of numerical and experiential for the 2024-T4 aluminum specimens is shown in Figure 12.31. The results were found to agree well with the existing experimental data. Figure 12.32 presents a series of predicted results for the bolt depression deformation under different loading stages. From the numerical results, the prediction is fairly good if the nonlinear material behavior is included in the model.

BG diagnostic system presents a more practical technique to the applications of structural health monitoring to bolted joints. Test results have shown that BG method in detecting the bearing damages can respond to change of parameters, such as material, initial clamping force, joint geometry and loading history.

References

- 1) Yi Xiao, Yoshiaki Kakuta and Takashi Ishikawa: Innovative Design of Mechanically Fastened Joints with Damage Diagnostic Function, *J. Jpn Soc Compos Mater*, 32(4), 2006, p.171.

2) Xiao, Y., Kakuta, Y. and Ishikawa, T.: A Design of Intelligent Bolted Composite Joints with Damage Detection Function, Proceedings of Annual Meeting of Japan Society for Composite Materials, 2003, p.63.

3) Yi Xiao, Yoshiaki Kakuta and Takashi Ishikawa: A self-diagnostic technique for monitoring the bearing damage in composite and metallic joints, Fifteenth international conference on composite materials, (2005), CD-ROM.

12.4.6 A-VaRTM for Primary Aircraft Structures

Yasuhiro Komori*, Fumihito Takeda*, Yasuo Suga**, Nobuo Asahara**

* Mitsubishi Heavy Industries, Ltd. (MHI)

** Toray Industries (Toray)

Advanced Vacuum-assisted Resin Transfer Molding (A-VaRTM) process for Carbon Fiber Reinforced Plastics has been under development aiming for application in aircraft primary structures. Since we use newly designed fabric and toughened resin system with efficiently designed resin infusion process, a superior mechanical strength has been realized. Also, several techniques have been developed by use of the advantage of dry pre-forming to achieve low cost and high produce-ability. To confirm the overall maturity of this technology, MHI and Toray have fabricated a proto-typed vertical stabilizer box assumed to be used on a regional jet type aircraft. This work is partially funded by New Energy Development Organization (NEDO) of Japan.

Fabrication Process

Low-cost dry fabrication, one of the key technologies in A-VaRTM, consists of:

- 1) Fully automated “Dry” pre-form fabrication
- 2) High quality drape capability which enables us to align with complex IML geometry such as skin

A uniform and straight cross section stringer has been developed shown in Figure 12.33. The trial product has been made by proto-typed machine.

Aggressive ply-drop-off test (including the ramp ratio 100:1, 50:1 and 25:1) shows great advantage of “Dry” process of A-VaRTM compared to “pre-impregnated based” process. Fiber wrinkle is one of the most significant factors to reduce part strength and stiffness. “Pre-impregnated based” process has a limitation with the large ramp ratio due to fiber wrinkling. In A-VaRTM process, however, no fiber-wrinkle is observed even with 25:1 ramp ratio shown in Figure 12.34, based on DI and NDI results.

Such quality improvement in A-VaRTM process is realized by not only dry process but also hot compaction process. Hot compaction process is a unique process in A-VaRTM to keep dimensional accuracy with the fiber volume control and the internal quality in dry pre-form. Also, we expect to utilize this hot compaction process to eliminate handling induced fiber wrinkle in dry pre-forming. This concept will realize easy in-process rework.

Proto-typed vertical stabilizer box structure

A-VaRTM technology has been matured based on good characteristics in the material, fabrication process and the strength / stiffness of structural components and the design concept and we can proceed to verify A-VaRTM technology by “Proto-typed Vertical Stabilizer” shown in Figure 12.35.

Design optimization for Proto-typed vertical stabilizer box structure has been conducted not only to withstand current load condition for a regional jet aircraft but also to select the low-cost fabrication process of parts without any significant risk. The structure box includes skin panels with co-bonded stringers, 2 spars and ribs by A-VaRTM material and process.

Finally, we can conclude that the proto-typed box shows the good prospect for applying A-VaRTM in primary structural elements.

12.5 FULL-SCALE TESTING

12.5.1 US-1A KAI Full-Scale Fatigue Test

M. Kageyama, M. Ito and H. Kawakami

Technical Research and Development Institute (TRDI), Ministry of Defense

The development of the US-1A KAI, Japanese new search and rescue amphibian aircraft, was started in 1996 for Japan Maritime Self Defense Force (Figure 12.36). The aircraft is modified on the base of current aircraft US-1A, and improvements are a pressurized cabin, replacement f engines, etc. The full-scale static test finished without any critical failure in primary structures in March 2005. The full-scale fatigue test (FSFT) has started since January 2004 by the TRDI Air Systems Research Center (formerly Third research center). The durability test of two-life-time loading was completed in the late 2004 as reported in the previous ICAF national reviews, and then the damage tolerance test of another two-life-time loading and the teardown inspection were carried out in early 2006. The main feature of the FSFT is as follows:

- Primary structures including fuselage, wing, landing gear and engine pylons except

for empennage not modified from the current aircraft

- Integration of landing gear fatigue test into the FSFT
- Flight-by-flight random loading spectra
- 167 hydraulic actuators and approximately 2000 strain gages

The test spectrum for the US-1A KAI consists of 9 mission types distributed over 7,500 flight lifetime based on each mission utilization rates. Each mission contains a specific ground, water and flight segment which has a specific weight, speed and altitude. Each flight segment in a mission profile has sub-segments such as a vertical gust, symmetric maneuver, ocean takeoff/landing, etc. Each sub-segment has a table of cumulative occurrences based on MIL specifications or the load experience of current aircraft.

The damage tolerant test was conducted to evaluate crack growth properties of modified sections from the current US-1A, where the slow crack growth design was primarily applied to those sections. More than 70 artificial flaws in consideration of MIL-A-83444 were applied to the test article. The results indicate that the crack growth rates were almost equal to or slower than numerical analyses and thus the damage tolerant design of the aircraft were valid.

12.5.2 P-X/C-X Full-Scale Structural Strength Test

M. Kageyama, M. Ito and H. Kawakami

Technical Research and Development Institute (TRDI), Ministry of Defense

TRDI now advances a joint development program of the next-generation maritime patrol aircraft (P-X) and the next-generation cargo aircraft (C-X) (Figures 12.37 and 12.38). P-X is the successor to the current Japan Maritime Self Defense Force's P-3C and also C-X is as to the current Japan Air Self Defense Force's C-1. Kawasaki Heavy Industries was selected as the prime contractor for the program. P-X has a low wing with four newly developed engines (XF-7) made by Ishikawajima-Harima Heavy Industries, and new maritime patrol combat systems. On the other hand, C-X equips two CF6 engines to high wing. The outer wings, a part of empennage and some equipment in the flight deck of the two aircraft are common to contribute to the life-cycle-cost reduction.

The full-scale static tests (FSST) and full-scale fatigue tests (FSFT) are planned for each aircraft. Both of test articles for the FSST were delivered in the late 2006, and the FSST is now ongoing (Figures 12.39 and 12.40). On the other hand, the test articles of the full-scale fatigue tests (FSFT) are in course of manufacture now. The objective of the FSFT is to evaluate all primary structure in order to demonstrate their capabilities to achieve the design service life goal for each aircraft. In detail, the full-scale test article is required to experience

two lifetimes of spectrum loading in each of the durability test and damage tolerant test. Primary structures consist of wing, fuselage, back-up structure for the landing gear, engine pylons, stores pylons and landing gear itself. Especially in this test, the main strut of the landing gear attached to the fuselage is tested together with fuselage. The load spectra simulate flight-by-flight utilization. The load cases comprise of maneuver, gust, landing, taxiing and cabin pressure.

12.5.3 Structural Substantiation of Unmanned Supersonic Experimental Airplane for Vibratory Loading

Shigeru Machida and Masahisa Honda

Japan Aerospace Exploration Agency (JAXA)

Japan Aerospace Exploration Agency (JAXA) is promoting the National Experimental Supersonic Transport (NEXST) program toward the development of the next generation SST.

On 10 October, 2005, the flight trial of the unmanned experimental plane was successfully conducted at Woomera Test Range, Woomera Prohibited Area, South Australia.¹⁾ (Fig. 12.41) The final goal of this flight test was to substantiate supersonic drag reduction technology with a CFD (Computational Fluid Dynamics)-based optimum aerodynamic design procedure and to establish the experimental system with the non-powered and unmanned supersonic experimental airplane (NEXST-1).²⁾

The NEXST-1 is the scaled airplane which has a length of 11.5m, a wing span of 4.7m, and about 2,000kg in weight. The airplane configuration was designed using the inverse method giving the preferable pressure distribution to minimize the aerodynamic drag force at Mach Number 2. Four concepts of the natural laminar flow (NLF) on the wing surface, the warp technology for wing twist, the cranked arrow wing plan form, and the supersonic area rule for fuselage shape were adopted in the aerodynamic design. A large number of sensors were installed to acquire data such as aerodynamic pressure, boundary layer characteristics, temperature, structural strain and acceleration during the flight.

Because of the limitation of the fuselage diameter, the landing gear was not equipped, whereas the recovery system, pilot-chute, drogue-chute and main parachute and airbags, were installed. The NEXST-1 had one solid rocket booster, NAL735. The weight was about 5,900kg. The booster and the NEXST-1 were connected by four separation bolts (Figure 12.42).

Figure 12.43 shows the structural layout of the NEXST-1 airplane. Inner wing of the

NEXST-1 has multi-spar box structure which is generally selected for delta wing shape. Outer wing, tail wings, ailerons and rudder were machined from aluminum plates because of their thin wing sections. Longeron concept, multi-frame and skin structure with longeron, has been adopted for the fuselage because of its low loading.

To satisfy the requirements from the unique mission, the following design conditions were applied.

- (1) Safety factor of 1.5 was used for static strength as well as civil aircraft.
- (2) Calculated flight loads were doubled for the design limit loads conservatively because of no experience of flight with the NEXST-1 before.
- (3) Vibratory loads from the solid rocket booster were conservatively estimated based on the data from static firing test of the rocket.
- (4) Temperatures of 230°C(446°F) at nose area and 200°C(392°F) at other section were considered for the structural design.
- (5) The airplane must be free from aeroelastic instability during the flight including launching phase.

Static strength of the airframe was substantiated by conducting a strain survey testing and analysis based on the test results. Since only two experimental flight per vehicle were planned, fatigue evaluation was not required. On the other hand, the airplane was subjected to vibratory loads from the solid rocket booster. These vibratory loads at frequency of 73Hz for 80 seconds are generated by flow-induced acoustic resonance of rocket motor case. As the results of structural response, these vibratory loads are critical for the separation units between the pilot-chute container and main parachute container (Figure 12.44). Fatigue (safe-life) evaluation was used for the substantiation. At first, P/N curve (loads vs. cycles) was generated from the fatigue tests in the laboratory with twelve separation units and scatter factor of 4.13 was calculated from test results based on 99 % probability with 95% confidence. The reduced P/N curve, applied the scatter factor on time scale, was used to evaluate the cumulative fatigue damage with Miner's Rule and the results showed that the separation unit was able to withstand the vibratory loads. After this evaluation, component fatigue tests with the actual separation units and the pilot-chute container were conducted and showed that the units was able to withstand the maximum vibratory loads for 30 minutes and more. Therefore sufficient fatigue strength of the separation units was substantiated. (Figure 12.45)

The flight trial was conducted successfully on 10 October, 2005 in Woomera Test Range. The total flight time was about 15 minutes and the NEXST-1 has made a perfect flight as

designed. The successful flight trial shows the substantiation of supersonic drag reduction technology with a CFD-based optimum aerodynamic design procedure.

From the structural point of view, this flight could show us the compliance with the structural design criteria, such as loadings, vibration, aeroelasticity and structural temperature.

References

- 1) Takeshi Ohnuki, Keiichi Hirako, Kimio Sakata, "National Experimental Supersonic Transport Project", ICAS 2006-1.4.1, ICAS2006, Hamburg, Germany, 3-8 Sep. 2006
- 2) Shigeru Machida, Kenji Yoshida, Takeshi Ohnumi., "Supersonic Flight Testing of Unmanned Experimental Airplane for Next-generation SST", AIAA-2007-854, 2007

12.6 STRUCTURAL HEALTH MONITORING

12.6.1 Structural Health Management of Composite Structures Using Small-Diameter Fiber Optic Sensors

Nobuo Takeda

The University of Tokyo

Optical fiber sensors are promising as tools for damage and structural health monitoring (SHM) of aerospace composite structures. The authors and Hitachi Cable, Ltd. have recently developed small-diameter optical fiber and its fiber Bragg grating (FBG) sensor for embedment inside a lamina of composite laminates without strength reduction. We are currently conducting the ACS-SIDE (Structural Integrity Diagnosis and Evaluation of Advanced Composite Structures) project on the optical fiber based SHM for some feasible applications in aerospace composite structures.

The ACS-SIDE project was established in 2003 as a five-year program by RIMCOF (Research Institute of Metals and Composites for Future Industries) and funded by METI (Ministry of Economy, Trade and Industries), Japan. The main goal of the project is to establish the following three structural health monitoring technologies for prototype applications in advanced aircraft composite structures.

(1) PZT/FBG hybrid sensing system for bond-line monitoring in CFRP box structures

A new hybrid and active sensing system with PZT actuators and FBG sensors was developed by our group. The main focus was laid on the bond-line monitoring (debonding at inaccessible bonded areas) in CFRP box structures during fatigue loading. Lamb waves generated by actuators can travel in some distance and are influenced by damaged or

debonded regions. Then, these Lamb waves were measured by a newly developed high-speed optical wavelength interrogation system. The delamination growth was successfully identified using the parameters derived from the change in the Lamb waves due to the debonding (Figure 12.46).

(2) Highly reliable advanced grid structures (HRAGS)

A grid structure made of CFRP unidirectional composites, named as an advanced grid structure (AGS), has specific characteristics such as simplicity of stress path /damage feature and fail-safe structural redundancy. We are proposing the HRAGS system equipped with a SHM system utilizing FBG sensors embedded in every rib of AGS so that the size and the intensity of operational or accidental damages can be evaluated through the strain measurement of every rib. A user-friendly and robust procedure to determine the damage location was developed for use in practical aircraft operating conditions (Figure 12.47).

(3) Distributed strain sensing using Brillouin optical correlation domain analysis (BOCDA)

Comparison of strain distribution between BOCDA and electrical strain gages was conducted in buckling tests of stiffened panels. A spacial resolution of 50 mm was demonstrated. The high-speed sampling at a certain point in an optical fiber was also demonstrated. Then, a demonstration flight test was conducted to obtain in-flight data and to understand some problems for use under practical flight conditions.

12.6.2 Structural Health Monitoring of Composite Wing Structure during Durability Test

S. Takeda*, Y. Aoki*, T. Ishikawa* and N. Takeda**

* Japan Aerospace Exploration Agency (JAXA)

** The University of Tokyo

One kind of the fiber-optic sensors, fiber Bragg grating (FBG) sensors were applied to a durability test of a composite wing structure. In order to verify the health monitoring capabilities for long-time use, strain fluctuation was measured by using a fiber Bragg grating swept laser interrogator (FBG-SLI) during the test continuously. This interrogator was 4-channels system that can monitor up to 256 gratings at more than 100Hz. The diameter of the FBG sensor with plastic coating was 150 μm , and the gauge length was 10 mm. All the sensor arrangements and impact locations are illustrated in Figure 12.48. In this research, the impact damages were also detected by the spectrum change in the FBG.

A linear relationship between the strain change and the wavelength shift of the spectrum is well known, and they have been applied to the strain measurement. Hence the relationship is

derived from the FBG sensors F2 and F5 experimentally, during a strain survey test within 40 % of the design limit load. The wavelength shift and the strain change measured by conventional strain gauges are shown in Figure 12.49. The locations of strain gauges SS118 and SC-121-11 correspond to FBG2 and FBG5, respectively. The strain change $\Delta\varepsilon$ is expressed as

$$\Delta\varepsilon = \frac{\Delta\lambda}{737.8} \quad (1)$$

where $\Delta\lambda$ is the wavelength shift. Using the equation (1), the strain monitoring of the test panel was conducted during the fatigue tests. Figure 12.50 shows the strain change measured by the FBG sensors and the strain gauges during a part of A-type flight. The tendencies of the strain changes measured by the FBG sensors were in good agreement with those measured by the corresponding strain gauges. The maximum strains during A-type flight are summarized in Table 12.2. The difference between the compressive strains measured by the FBG sensor (F6) and the corresponding strain gauge (SC120-2) was investigated, because the calibration of the strain carried out using the strains measured by F2 and F5 during the strain survey test.

In order to detect barely visible impact damage (BVID) on point A, the FBG sensor (F1) was attached to the backside of the impact point A using the commercial strain gauge cements (see Figure 12.51 (a)). The measured spectra before and after the impact test were shown in Figure 12.51 (b). Though the spectrum has one peak before the impact loading, the shape of the spectrum is severely distorted after the impact loading. The change in the spectrum was caused by the complicated damages around the FBG sensor. Considering the shape of the spectrum, we can predict that cracks penetrate to the stringer flange, because the cracks easily occur along the loading (thickness) direction under the transverse impact loading condition. That is why the previous study has been reported that the width of the spectrum was broadened by the damages progressed perpendicular to the FBG sensor^{1, 2)}. Thus, the FBG sensor could detect the cracks prior to the delaminations among the BVID. After the impact tests, the BVID was observed by the pulsed heating thermography and the ultrasonic C-scan as shown in Figure 12.52. Since these results also indicate the complicated damages including the delaminations, the spectrum change of the FBG sensor was useful signal for the impact damage detection.

References

1) Okabe Y., Mizutani T., Yashiro S. and Takeda N., *Composites Science and Technology*, 62 (2002), pp. 951-958.

2) Mizutani T., Okabe Y. and Takeda N., *Smart Materials and Structures*, 12 (2003), pp. 898-1651.

12.7 AIRCRAFT ACCIDENT INVESTIGATION

12.7.1 Aircraft Accident Investigation and Aircraft Serious Incident Investigation

Kazushige Daiki, Aircraft and Railway Accidents Investigation Commission (ARAIC)

(1) Total number of registered aircraft in Japan

As of December 31, 2006, the number of registered civil aircraft in Japan was 2,663. This accounts for 1,217 airplanes (of which 586 airplanes with reciprocating engines), 778 helicopters, 665 gliders inclusive of motor gliders and 3 airships.

(2) Statistics in relation to the accident and serious incidents investigation

The number of accidents and serious incidents which ARAIC investigated in the past two years are shown in Tables 12.3 and 12.4. Of the total 60 occurrences, 15 are still under investigation. Of the 45 published accident/incident investigation reports, pilot and maintenance related causes accounted for 58% and 16% respectively. Other causes such as weather conditions or undetermined, accounted for remaining 26%.

(3) Fatigue failure related accident

a. Summary of the accident

On Tuesday September 14, 2004, a McDonnell Douglas MD900 operated by Aero Asahi Corporation, registration JA6757, was on a return flight to Tokyo Heliport. Around 10:07 Japan Standard Time the aircraft lost yaw control, followed by No.2 engine failure. The aircraft tried to make an emergency landing at Atsugi airfield (RJTA) around 11:21, however, ended up a hard landing at west apron of the airfield. The aircraft sustained substantial damage. A tension-torsion (T-T) strap, which is a part of NOTAR® fan assembly and is used for changing NOTAR fan blade pitch was found fractured.

b. NOTAR system

NOTAR was invented to substitute conventional tail rotor. NOTAR fan housed in the aft fuselage pushes large amount of low pressured air into the tail boom. The air is released through slits cut in the right side of the tail boom and jet thruster. The air released through the slits flows along the tail boom surface by Coanda effect. Under the effect of main rotor downwash, tail boom acts like a wing and produces lift toward right when observed from aft and this becomes a part of anti-torque.

c. Construction of a T-T strap

A T-T strap (Figure 12.53) is a composite material which is made of Kevlar49 fibers continuously wound around two corrosion-resistant metal spools and impregnated in polyurethane. The outer surface is coated with polyurethane.

d. Cause of the T-T strap fracture

The probable cause of the rupture of T-T strap is estimated that repetitive large compression and shear strain generated in the area where T-T strap composite material is closest to the edge of the spool, was not considered at the time of its design, lead to fatigue of the material from that area and degraded the strap's integrity.

12.8 ICAF DOCUMENTS DISTRIBUTED BY JAPAN DURING 2005 TO 2007

- (1) Enhancement of Mechanical Strength by Shape Memory Effect in TiNi Fiber-Reinforced Composites, *Engr. Frac. Mech.* 71 (2004), pp. 737-746 (A. Shimamo, H. Ohkawara, F. Nogata)
- (2) Numerical Simulation Study of Fatigue Crack Growth Behavior of Cracked Aluminum Panels Repaired with a FRP Composite Patch Using Combined BEM/FEM, *Engr. Frac. Mech.* 72 (2005), pp. 2549-2563 (H. Sekine, B. Yan, T. Yasuho)
- (3) Durability Analysis and Structural Health Management of Smart Composite Structures Using Small-Diameter Optic Sensors, *Sci. Engr. Compos. Mater.*, 12 (2005), pp. 1-12 (N. Takeda, Y. Okabe)
- (4) Development of Smart Composite Structures with Small-Diameter Fiber Bragg Grating Sensors for Damage Detection: Quantitative Evaluation of Delamination Length in CFRP Laminates Using Lamb Wave Sensing, *Compos. Sci. Tech.*, 65 (2005), pp. 2575-2587 (N. Takeda, Y. Okabe, J. Kuwahara, S. Kojima, T. Ogisu)
- (5) Estimation of the Damage Patterns in Notched Laminates with Embedded FBG Sensors, *Compos. Sci. Tech.*, 66 (2006), pp. 684-693 (N. Takeda, S. Yashiro, T. Okabe)
- (6) Structural Health Monitoring of Composite Wing Structure During Durability Test, *Compo. Struc.*, 79 (2007), pp. 133-139 (S. Takeda, Y. Aoki, T. Ishikawa, N. Takeda, H. Kikukawa)

ACKNOWLEDGEMENTS

The editors appreciated the members of the ICAF national committee of Japan Society for Aeronautical and Space Sciences, for their contribution in preparation of this national review and continuing discussion in the committee.

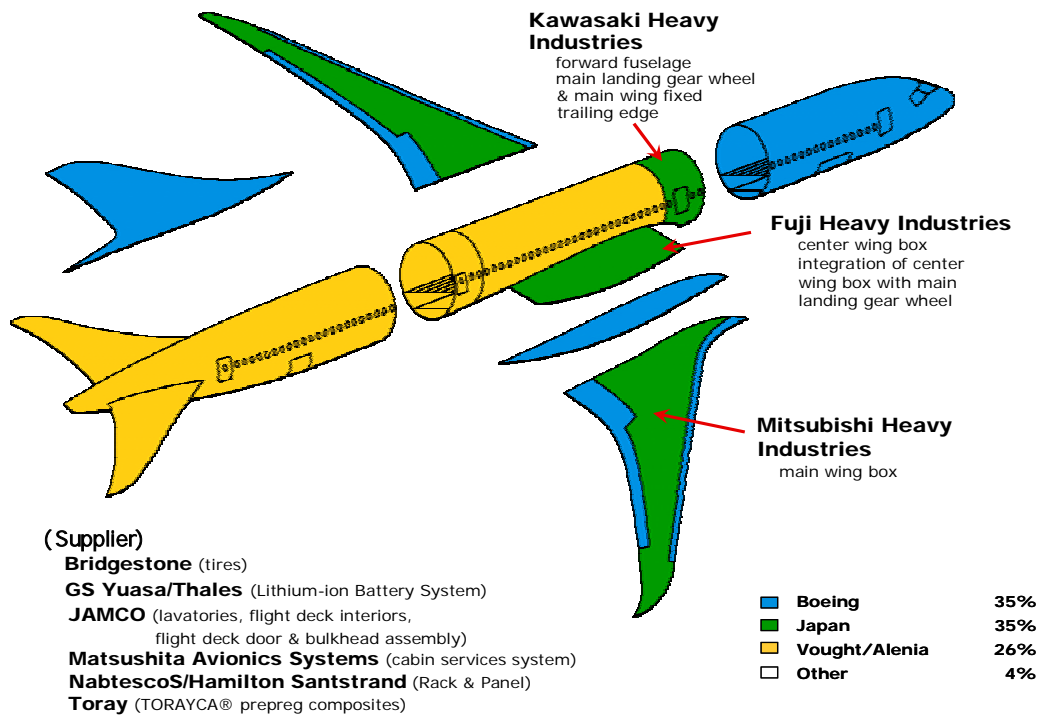


Figure 12.1 Structural Share Map of Boeing 787 Project

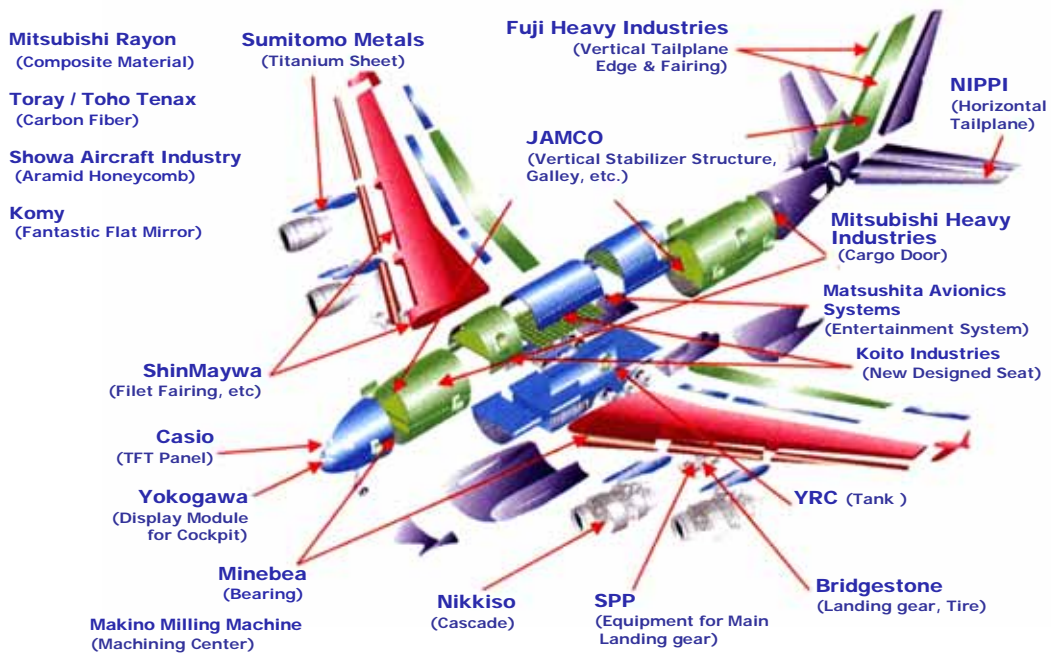


Figure 12.2 Parts of A380 Supplied from Japanese Industries



Figure 12.3 Image of Regional Jet Aircraft MJ90

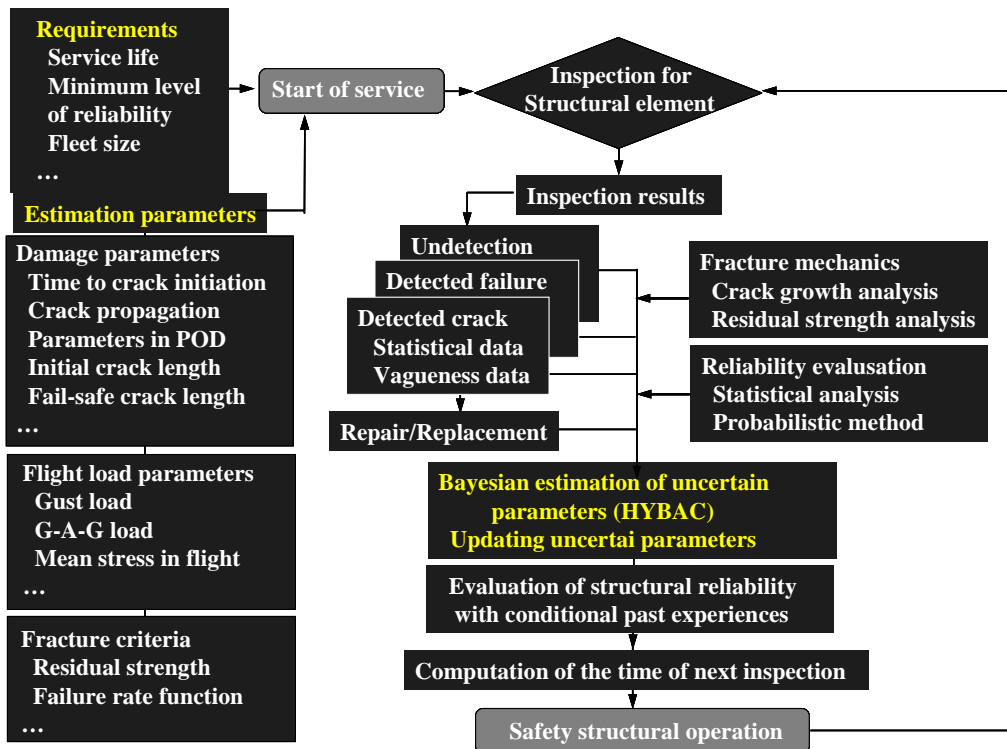


Figure 12.4 Methodology of HYBAC for Wing Surface Structure (Example)



Figure 12.5 Section Perpendicular to the Welding Line

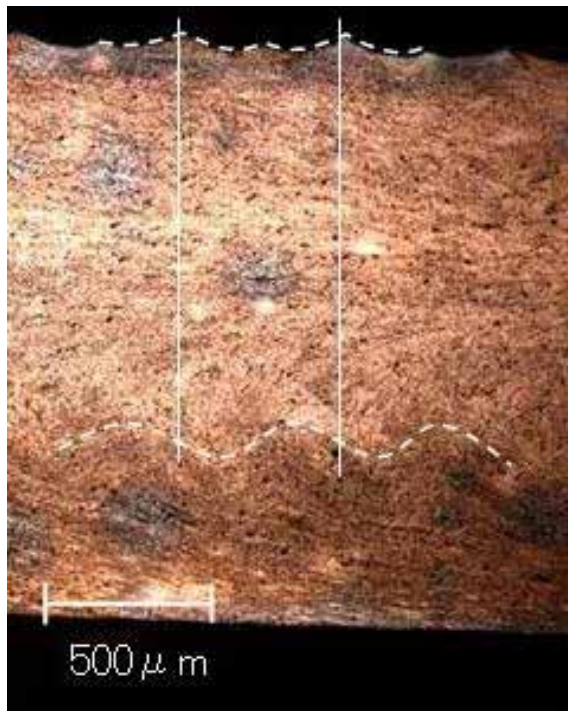


Figure 12.6 Section Parallel to the Welding Line



Figure 12.7 Five Stringer Panel

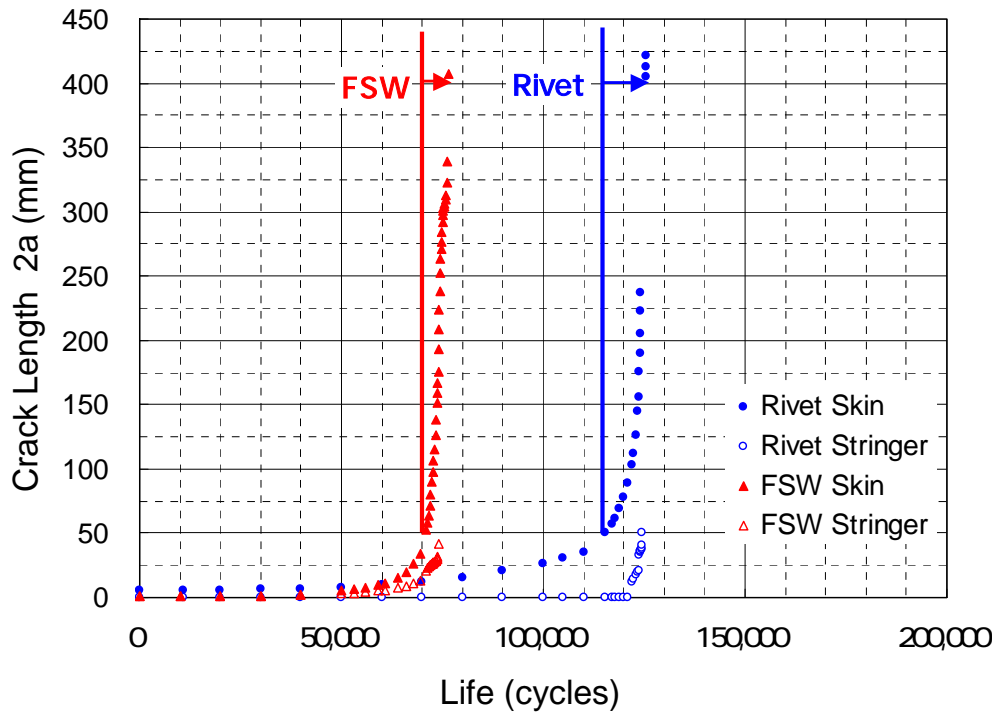


Figure 12.8 Crack Propagation Properties of FSW and Riveted Panels

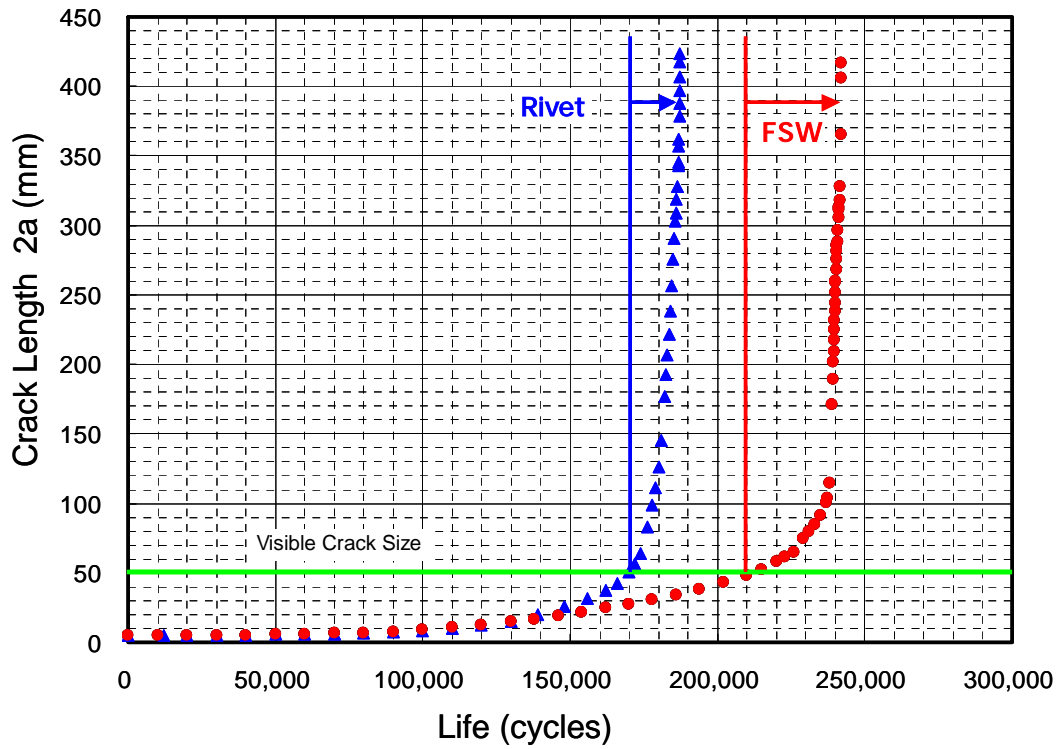


Figure 12.9 Crack Propagation Properties of Roller Burnished FSW Panels

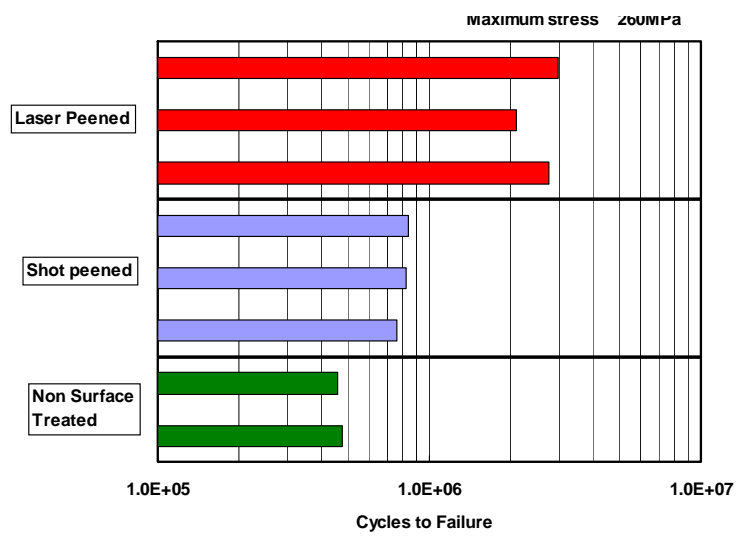
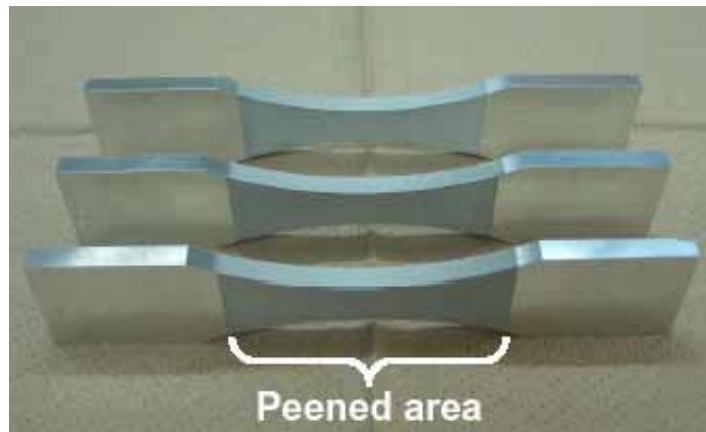


Fig. 12.10 Un-notched Coupon Test

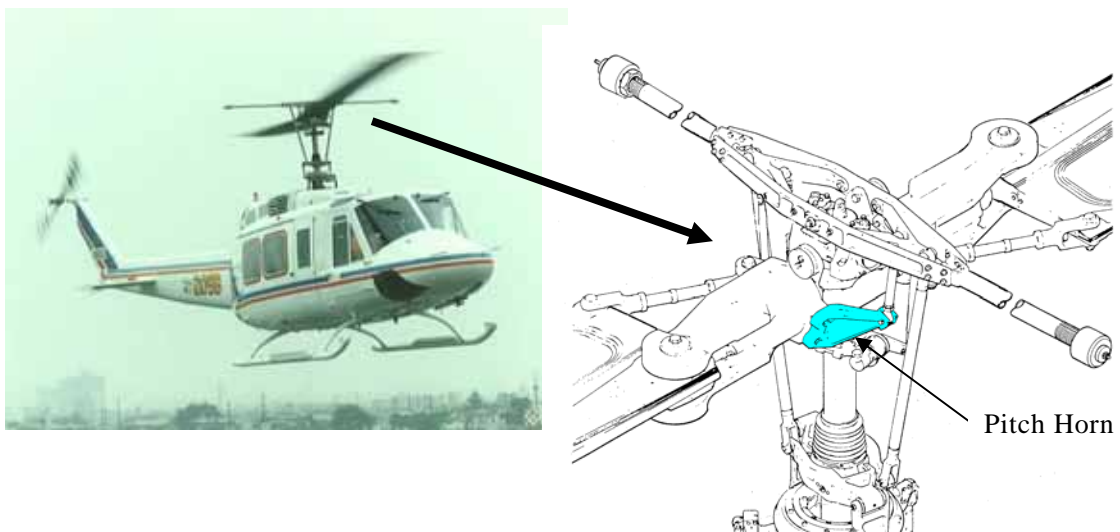


Figure 12.11 Pitch Horn of Helicopter



Figure 12.12 Actual-Sized Element Test (Pitch Horn)

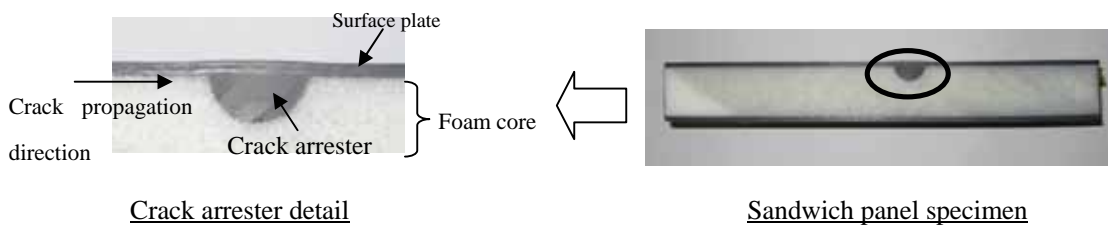


Fig. 12.13 Crack Arrester Concept

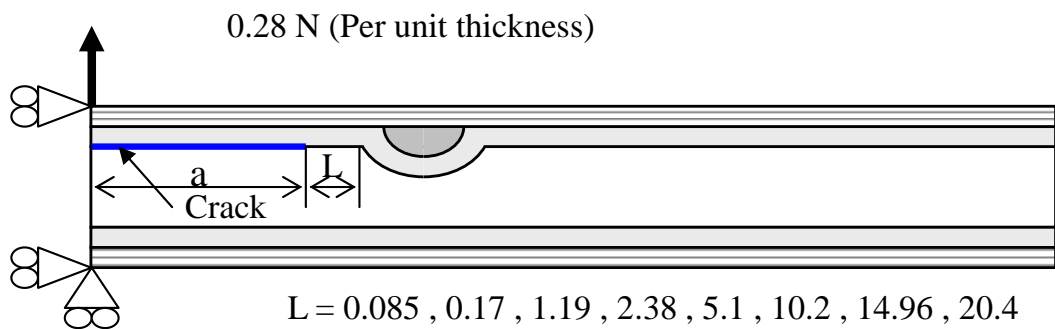


Fig. 12.14 Loading Condition of the Test Specimen

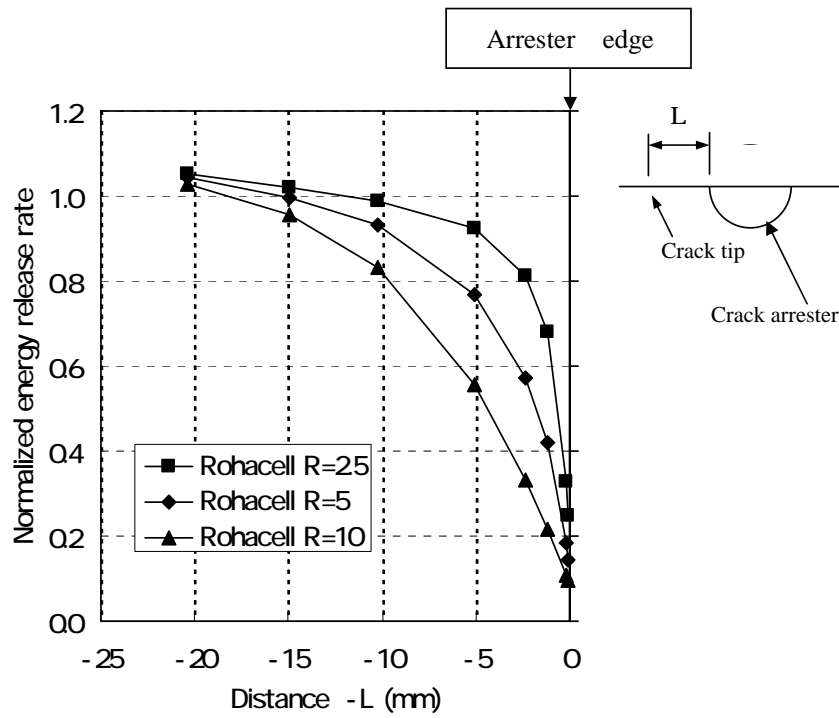


Fig. 12.15 Relation between Energy Release Rate G and Distance L for Mode I Type

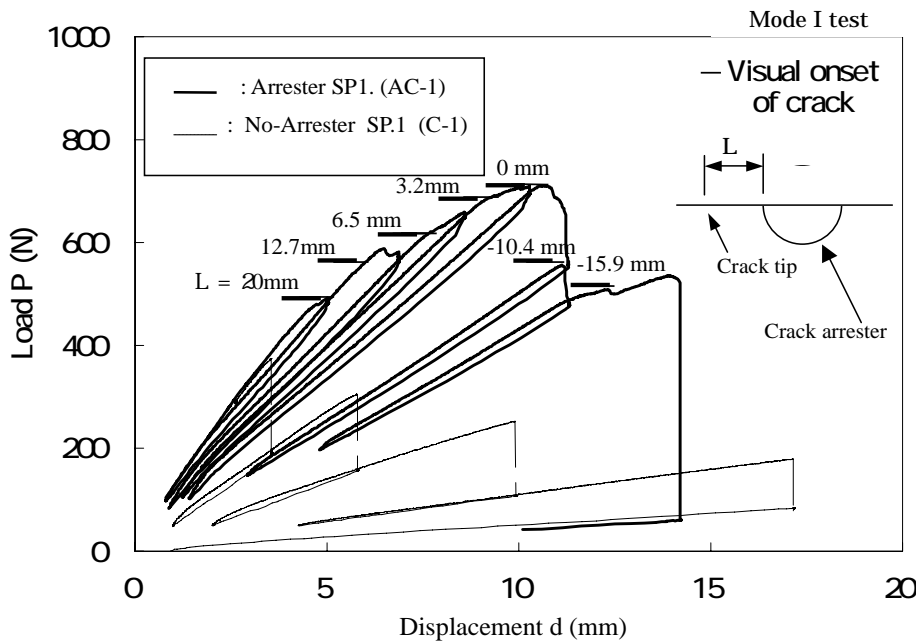


Fig. 12.16 Relation between Critical Load and Cross Head Displacement

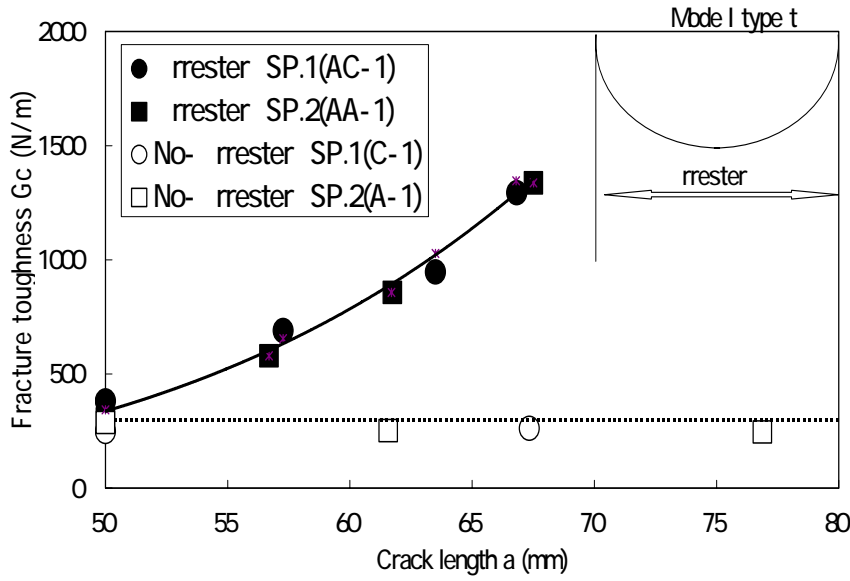


Fig. 12.17 Relation between Energy Release Rate and Crack Length

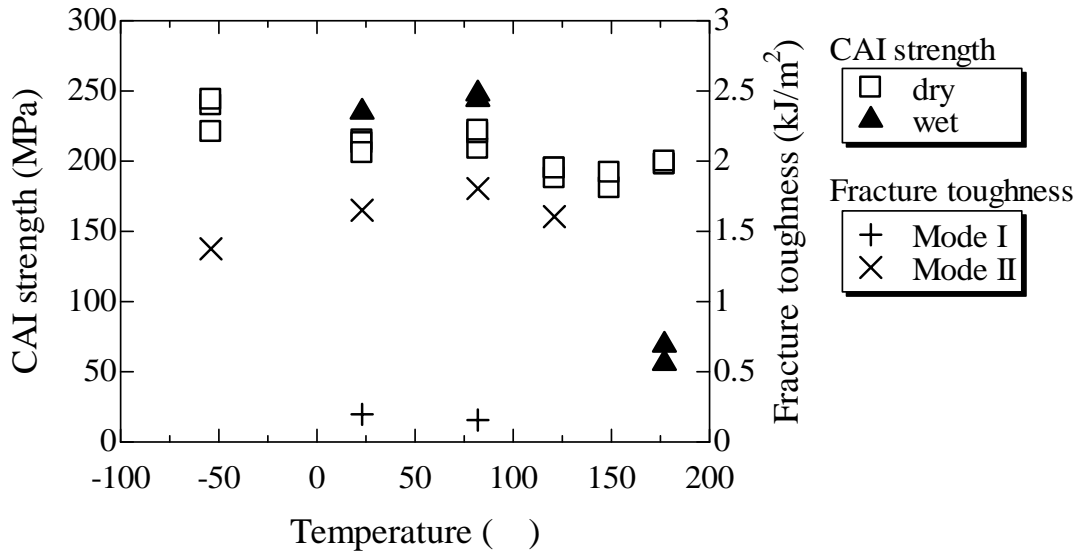


Figure 12.18 Relationships between CAI strength, Interlaminar Fracture Toughness and Temperature for T800/3633 CFRP Laminates

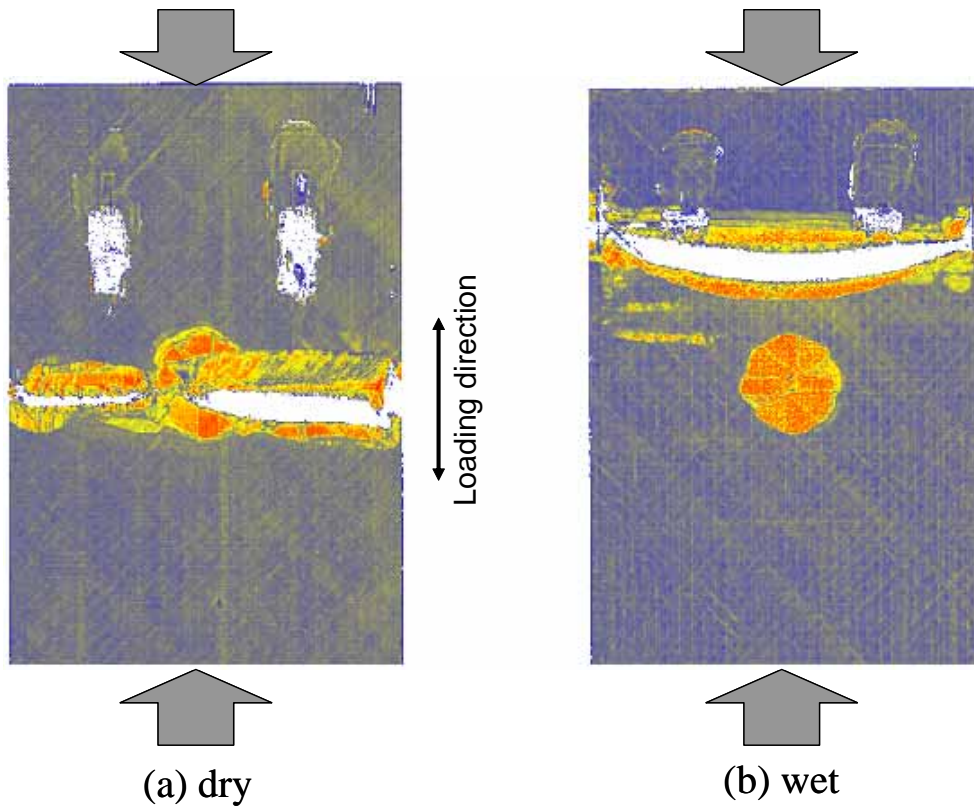


Figure 12.19 Ultrasonic C-scan Images Taken after Compression Tests at 177

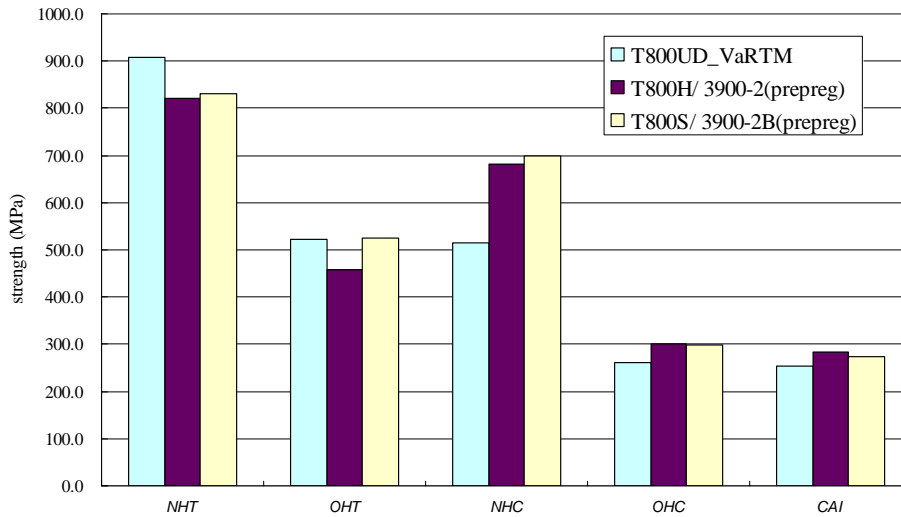


Figure 12.20 Results of Mechanical Properties of VaRTM Graphite/Epoxy Composites and Conventional Aircraft Grade Prepreg Composites



a) 2m stiffened panel



b) 2.1m long demonstrator



c) 6m long demonstrator

Figure 12.21 Three Types of Demonstrators Manufactured by VaRTM Process

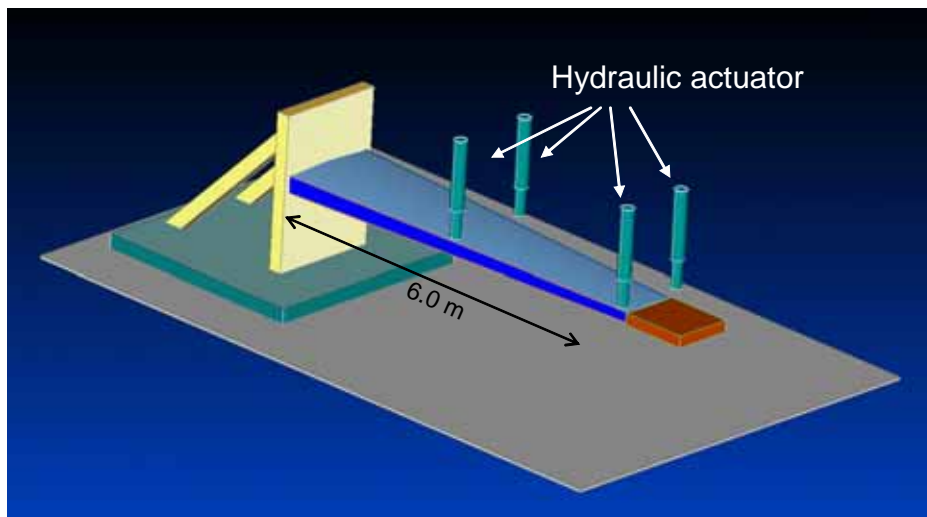


Figure 12.22 Experimental Setup of Full-scale Static Test of Wing Box

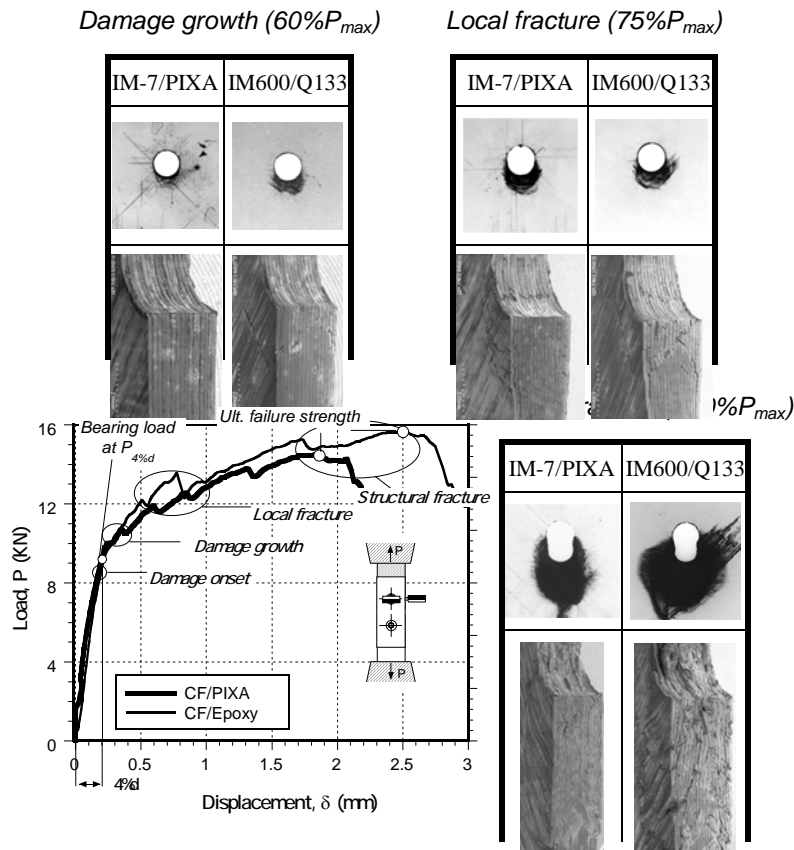
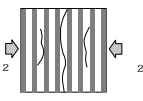
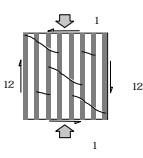


Figure 12.23 Relationship between Bearing Response and Damage Progression for IM-7/PIXA and IM600/Q133 Composite Joints.

Table 12.1 Failure Criteria and Damage Variable Applied to Progressive Damage Analysis

Failure mode	Failure index	Damage variable
 <p>Matrix compression failure</p>	$\sigma_2 \leq 0,$ $e_m^2 = \left(\frac{\sigma_2}{Y_c}\right)^2 + \left(\frac{\sigma_{12}}{S_c}\right)^2 \quad (3)$ <p>Hashin failure criteria</p>	$FV_1 \Rightarrow D_2, D_6$
 <p>Fiber compression-shear failure</p>	$\sigma_1 \leq 0,$ $e_{fs}^2 = \left(\frac{\sigma_1}{X_c}\right)^2 + \left(\frac{\sigma_{12}}{S_c}\right)^2 \quad (4)$ <p>Yamada-Sun failure criteria</p>	$FV_2 \Rightarrow D_1, D_2, D_6$

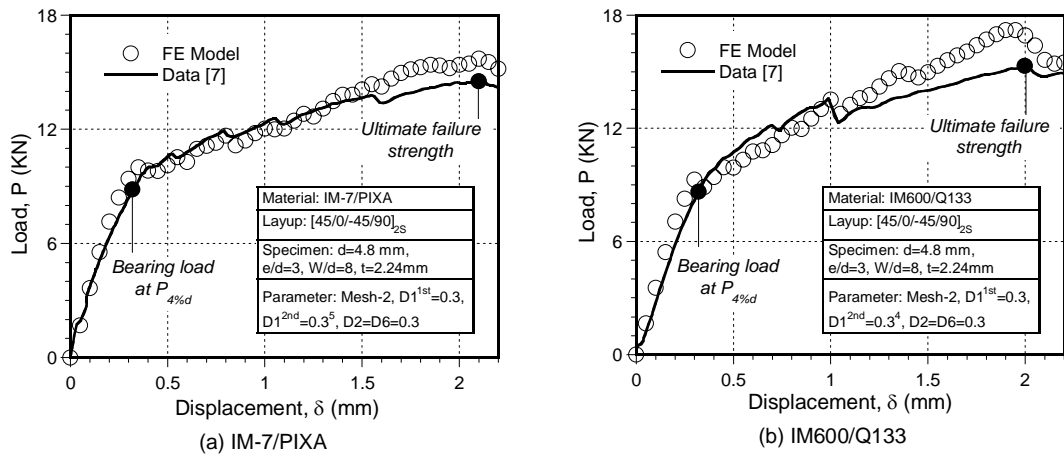
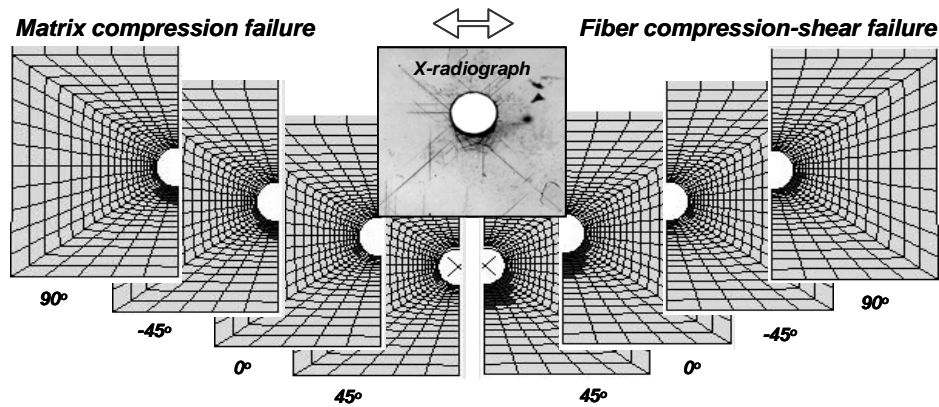


Figure 12.24 Comparison between Measured and Calculated Load-Displacement Curves for Two materials

(a) Load: P=10KN



(b) Load: P=16KN

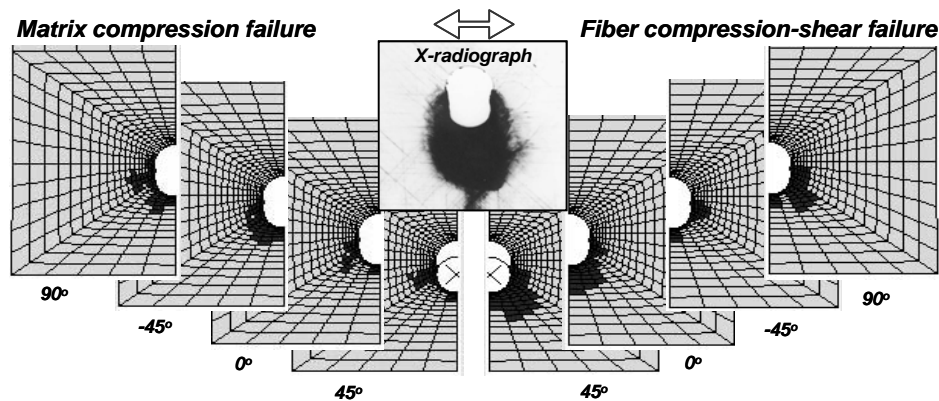


Figure 12.25 Comparison between X-ray Radiography and Numerical Damage Progression for the IM-7/PIXA [45/0/-45/90]_{2S} Laminate (a) P=10 kN, (b) P=16 kN

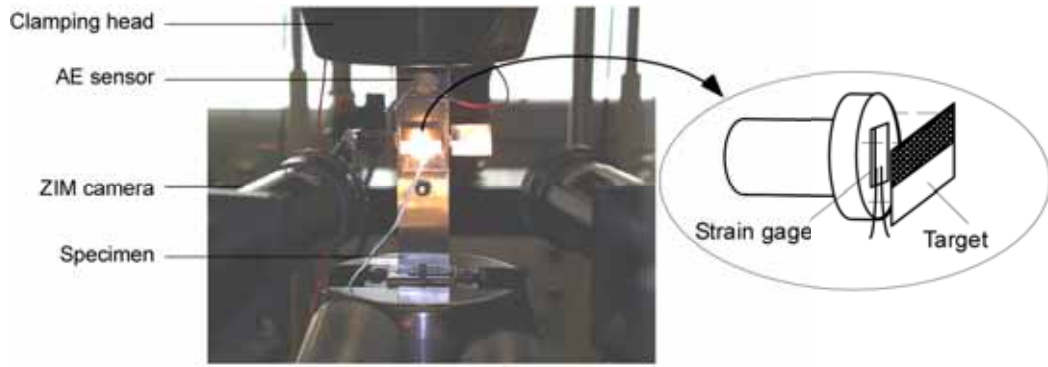


Figure 12.26 Schematic of Double Lap Joint Specimens with BG System

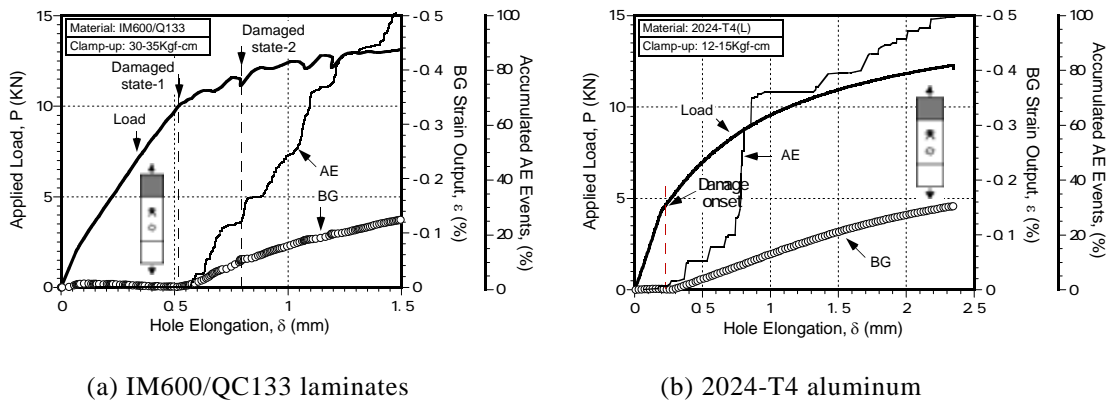


Figure 12.27 GB Responses for Different Material Systems Tested at Monotonic Tensile Loading

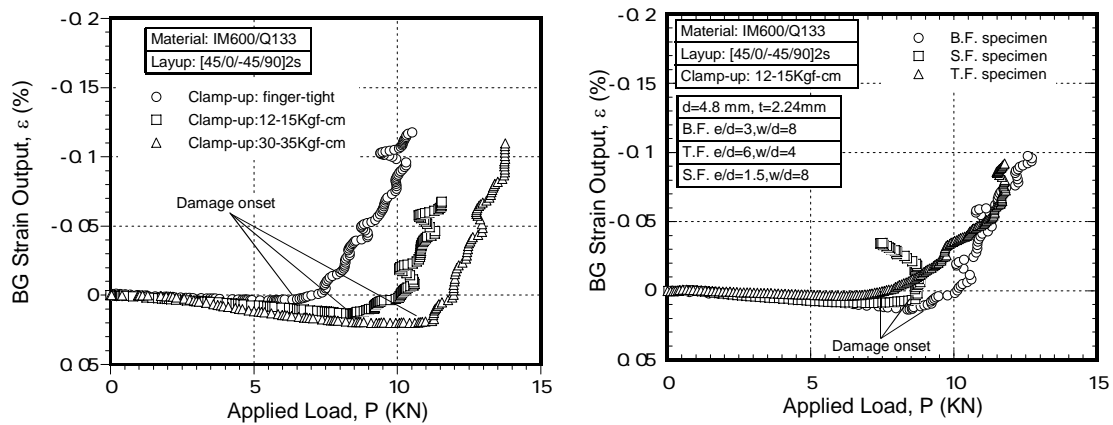


Figure 12.28 GB Responses Plotted as a Function of Applied Load for Different Clamping Forces

Figure 12.29 GB Responses Plotted as a Function of Applied Load for Different Joint Geometries

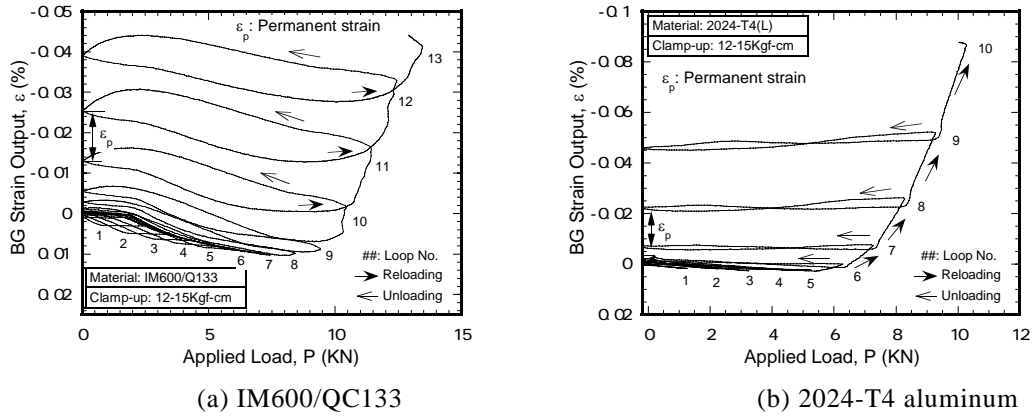


Figure 12.30 GB Responses Plotted as a Function of Applied Load Tested at Cyclic Loading/Unloading

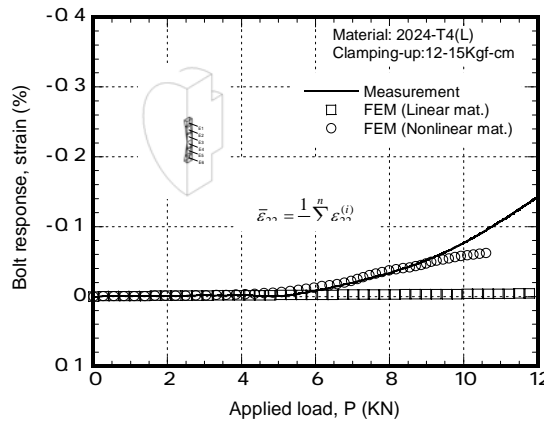


Figure 12.31 Comparison between Measured and Calculated BG Responses

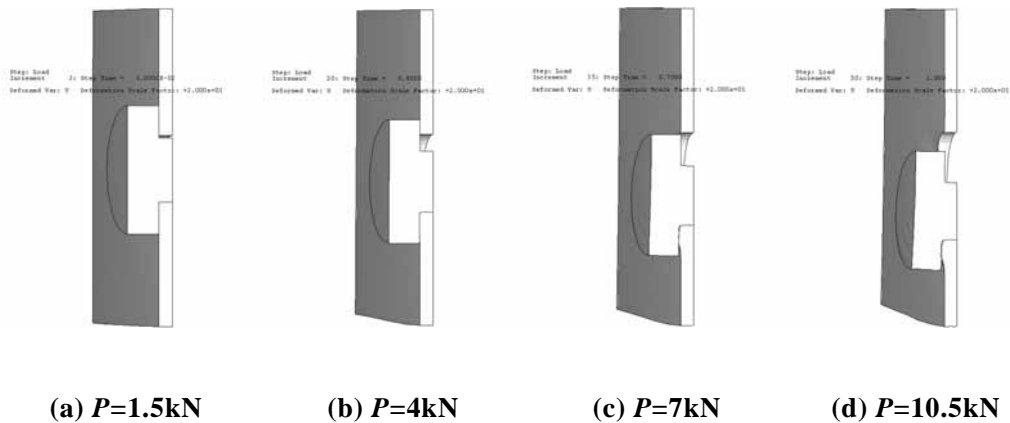


Figure 12.32 Predicted Bolt Depression Deformation

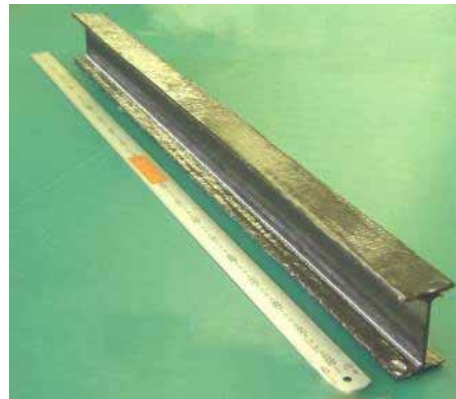


Figure 12.33. Stringer Dry Pre-form

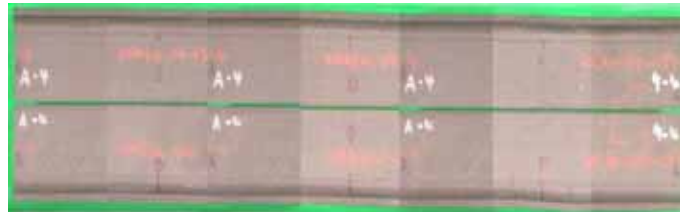
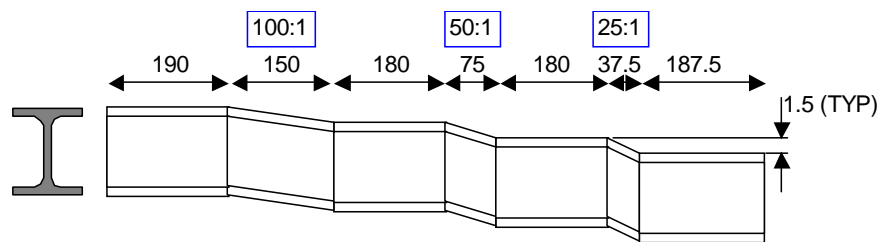


Figure 12.34. Ply Drop-off Condition



Figure 12.35 Proto-Typed Vertical Stabilizer Box Structure



Figure 12.36 US-1A KAI



Figure 12.37 P-X



Figure 12.38 C-X



Figure 12.39 P-X FSST Test Article



Figure 12.40 C-X FSST Test Article



Figure 12.41 Launching

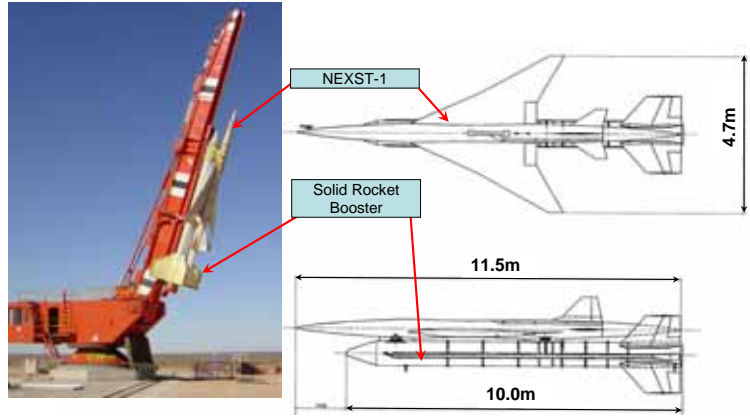


Figure 12.42 Experimental Airplane System

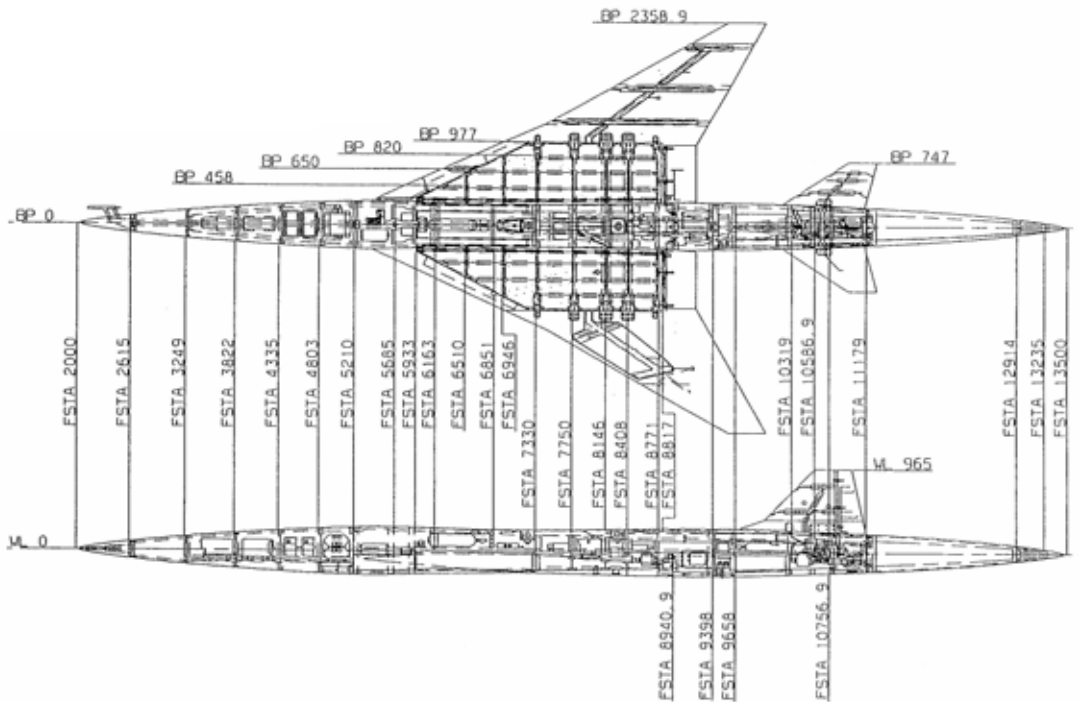


Figure 12.43 Structural Layout of the NEXST-1

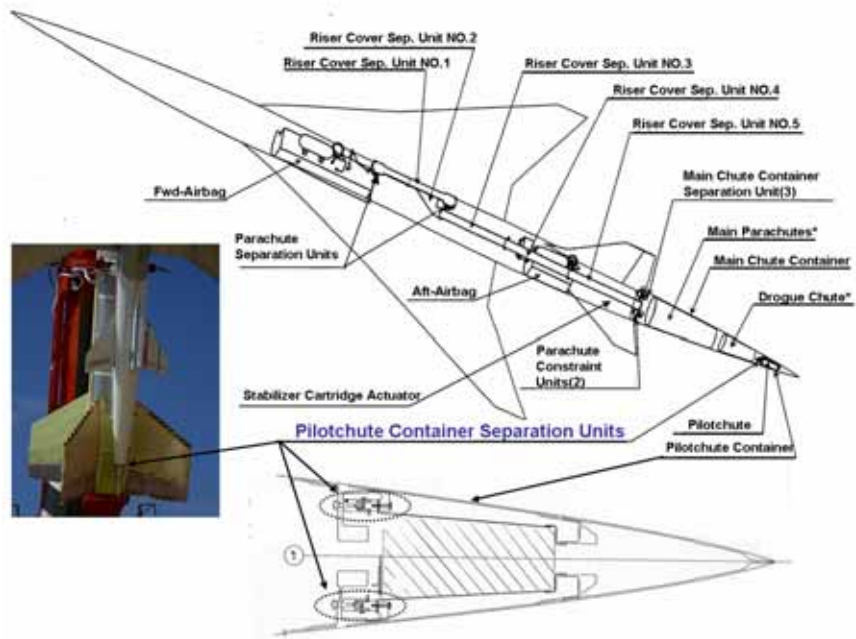


Figure 12.44 Pilot-chute Container Separation Units



Figure 12.45 Component Fatigue Test

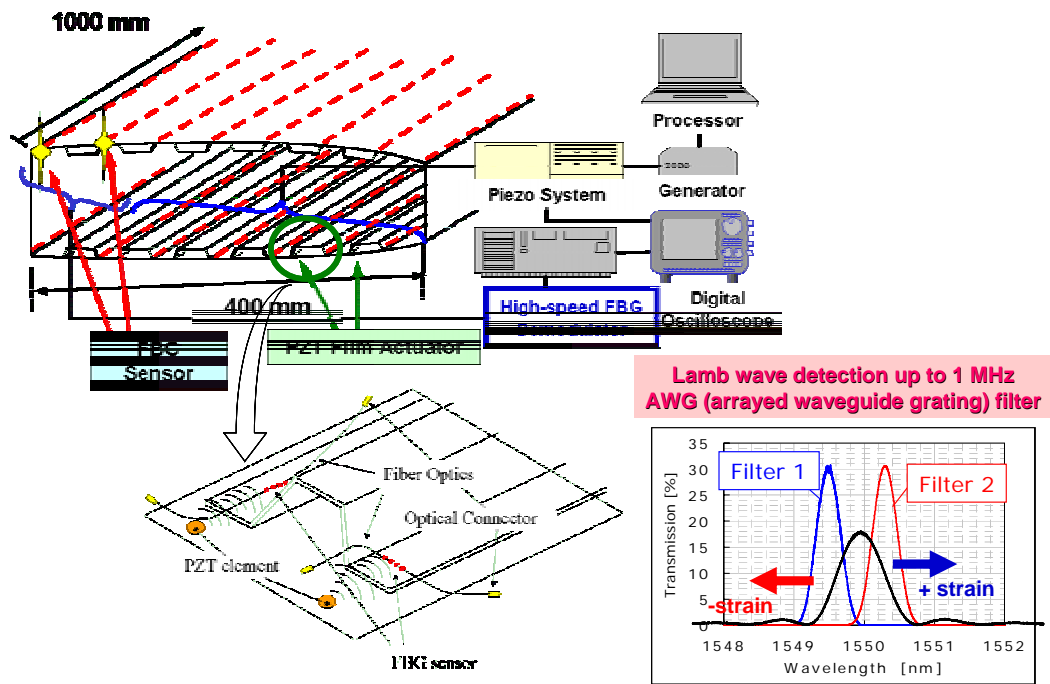


Figure 12.46 PZT-FBG Hybrid Active Damage Sensing System

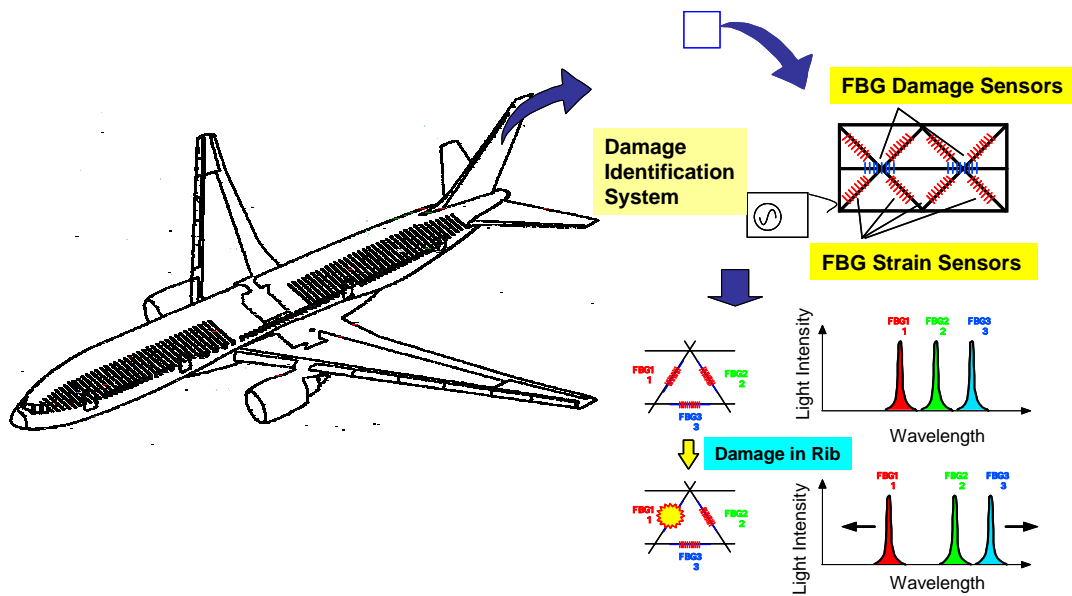


Figure 12.47 High Reliability Advanced Grid Structures (HRAGS)

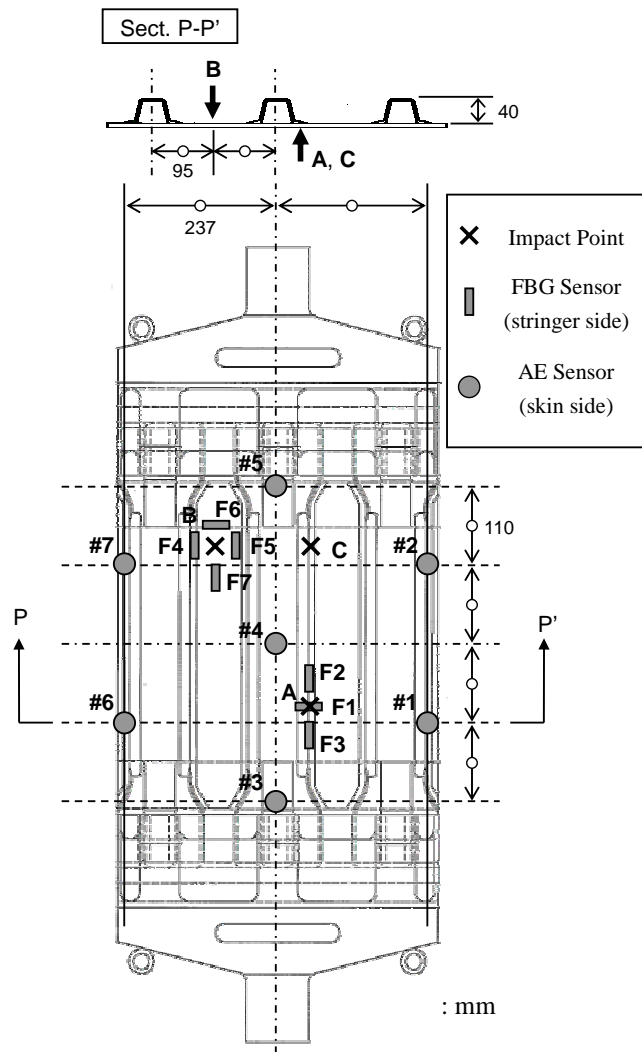


Figure 12.48 Illustration of Impact Locations and Sensor Arrangements

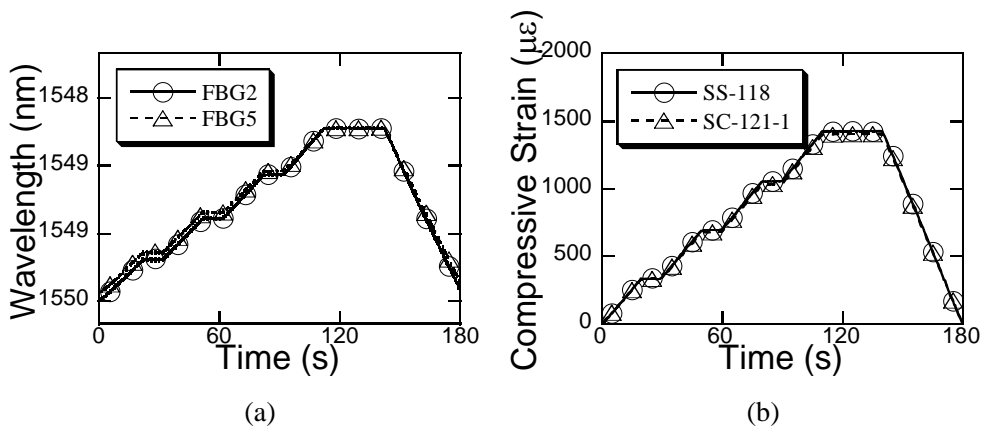


Figure 12.49 Relationship between Signal changes during a Strain Survey Test. (a) Wavelength shift and (b) compressive strain. FBG2 and FBG5 (b) correspond to SS118 and SC-121-1, respectively.

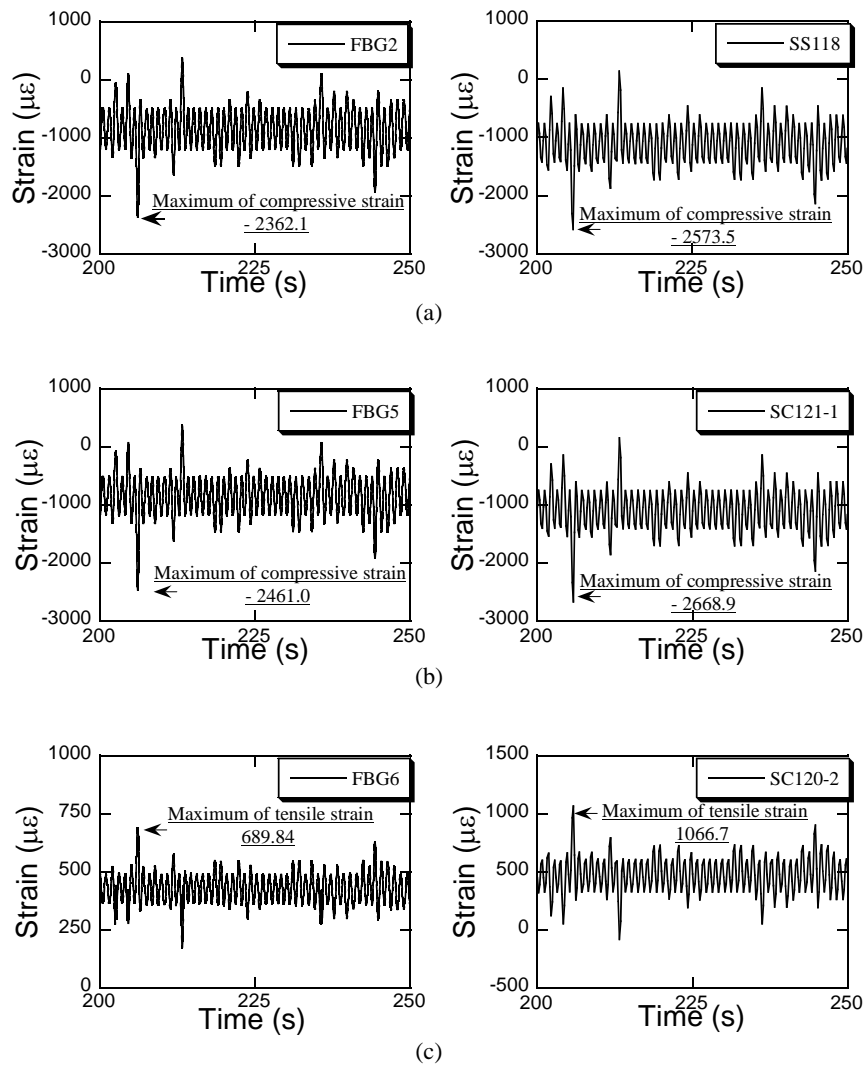


Figure 12.50 Strain Monitoring during a Part of A-type Flight. (a) FBG2, (b) FBG5 and (c) FBG6 correspond to SS118, SC-121-1 and SC120-2, respectively.

Table 12.2 Maximum Strains during A-type

	Strain ($\mu\epsilon$)	
	FBG Sensor	Strain Gauge
FBG2 (SS118)	- 2362.1	- 2573.5
FBG5 (SC121-1)	- 2461.0	- 2668.9
FBG6 (SC120-2)	689.8	1066.7

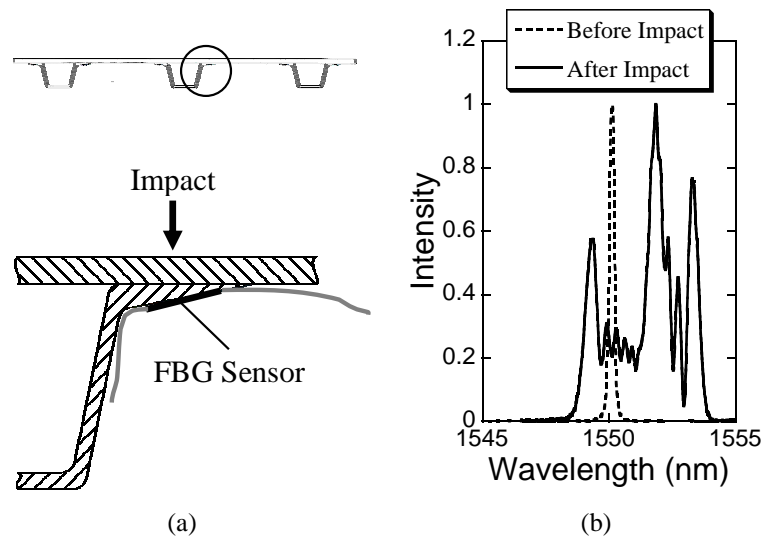


Figure 12.51 Detection of Impact Damages. (a) Sensor Attachment and (b) Spectra before and after Impact Test

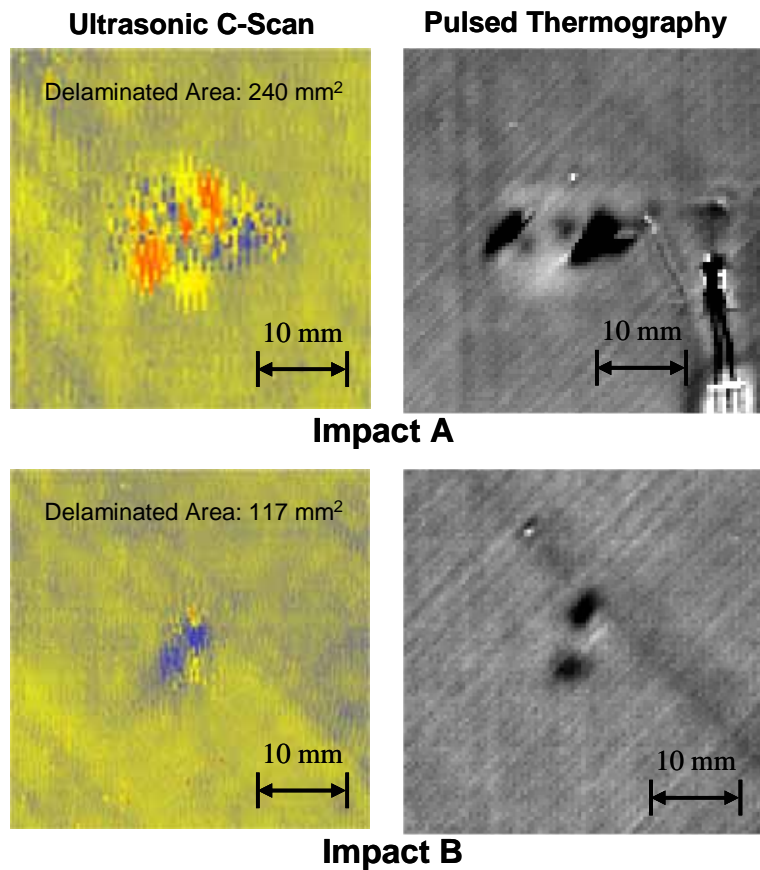


Figure 12.52 Photographs of BVID after Fatigue Tests (= 80,000 Flights)



Figure 12.53 T-T Straps

Table 12.3 Number of Accident Causes by Factor

Year \ Category	Pilot	Maintenance or material	Weather or other reasons	Still under investigation	Total
2005	13	2	6	2	23
2006	9	1	2	6	18

Table 12.4 Number of Incident Causes by Factor

Year \ Category	Pilot	Maintenance or material	Weather or other reasons	Still under investigation	Total
2005	4	3	4	4	15
2006	0	1	0	3	4